Ore Geology Reviews 91 (2017) 133–152

Contents lists available at ScienceDirect

Ore Geology Reviews

journal homepage: www.elsevier.com/locate/oregeorev

New metallogenic model of telescoped Eocene-Miocene Au-U epithermal mineral deposit in the Placer de Guadalupe district, Chihuahua, Mexico

Gilles Levresse[a,*], Janet Villarreal-Fuentes[a], Angel F. Nieto-Samaniego[a], Paul Alexandre[b], Rodolfo Corona-Esquivel[c], Jesus Solé Viñas[c]

[a] Centro de Geociencias, Universidad Nacional Autónoma de México, Blvd. Juriquilla No. 3001, Querétaro 76230, Mexico
[b] Queens University, Ontario, Canada
[c] Instituto de Geología, UNAM, Ciudad Universitaria, Mexico

ARTICLE INFO

Keywords:
Mexico
Au-U epithermal deposit
U dating
Telescoped deposit
Miocene

ABSTRACT

The chronological repartition of mineral deposits in Mexico and the southern USA coincides with the distribution of the three main volcanic pulses of the Sierra Madre Occidental. These pulses are Eocene to early Miocene in age, suggesting that a broad migration occurred from northwest to southeast, where the last ignimbrite flare-up occurred. The most fertile event occurred from 36 to 28 Ma and produced all of the largest Ag-Au mining districts. The Placer de Guadalupe Au-U district contain a unique association of metals with high variations in their U/Au ratios that are not common worldwide. The uraninite population dated by Wells (1930) yielded an age of ca. 36 Ma, which is comparable to that of the volcanic intrusions and dykes dated in the district (yielding ages of ca. 36 Ma). Altered uraninite cemented by gold sheets provide an age of 21 Ma, which is interpreted to be the age of the gold epithermal event. Studies of fluid inclusions in the quartz and calcite cements formed in the gold event indicate the presence of immiscible magmatic brines and CO_2. Homogenization temperatures by halite melting range from 268 °C to 305 °C and 266.6 °C to 283 °C, with salinities ranging from 35.9 to 38.9 and 36.0 to 37.5 wt% eq NaCl, in the quartz and calcite stages, respectively. C-O isotopic compositions of U and Au calcite cements suggest a trend of low-temperature alteration caused by hydrothermal fluids. These C-O isotopes suggest that during the gold event, water/rock interaction processes occurred between magmatic fluids and the carbonate host-rock. REE enrichment in the U calcite cement suggests that La-Ce enriched carbonatite volcanic formations participated in the mineralizing process. The U mineralization event was controlled by (1) a metal and heat source (in this case, late Eocene volcanism and, in particular, a carbonatite volcanic event); (2) an efficient transport mechanism for the large-scale input of meteoric water, which was channeled, heated and U-enriched into reactivated crustal Eocene faults from a deep U source to a shallow sedimentary chemical trap; (3) an effective trap, which is represented in this study by the presence of an organic matter-rich sedimentary formation. The gold mineralization event was characterized by the Miocene extensional peak coupled with asthenospheric upwelling, which facilitated the melting/metamorphism of the lower crust and the expulsion and transport of large amounts of CO_2-bearing fluids to a shallow crustal level through the reactivated crustal Laramide thrust faults. The fluids' interactions with the entire stratigraphic column, from the Grenvillian to the Late Triassic basement, favored the leaching of gold and the enrichment of CO_2-bearing fluids. Gold deposition appears to be related to boiling but was ultimately favored by water-rock interaction with U mineralization and the Upper Plomosas shale. Study of the Au-U Placer de Guadalupe deposit reveals evidence of a new Miocene metallogenic event in central and northern Mexico. Its genetic relationship with the Basin and Range (BnR) and Rio Gande Rift (RGR) in USA and its transition from post-orogenic to Miocene intraplate extension in Mexico provides a new perspective regarding the exploration of Miocene gold epithermal deposits in northern Mexico and the southern USA.

1. Introduction

The spatiotemporal distribution of hydrothermal, skarn, porphyries and orogenic gold deposits in Mexico and Arizona has been the subject of various studies over the last decade (Campa and Coney, 1983; Clark and Salas, 1988; Clark, 1997; Clark and Fitch, 2005, 2009; Camprubi

* Corresponding author.
E-mail addresses: glevresse@gmail.com, glevresse@geociencias.unam.mx (G. Levresse).

http://dx.doi.org/10.1016/j.oregeorev.2017.10.011
Received 31 March 2017; Received in revised form 10 October 2017; Accepted 13 October 2017
Available online 21 October 2017
0169-1368/

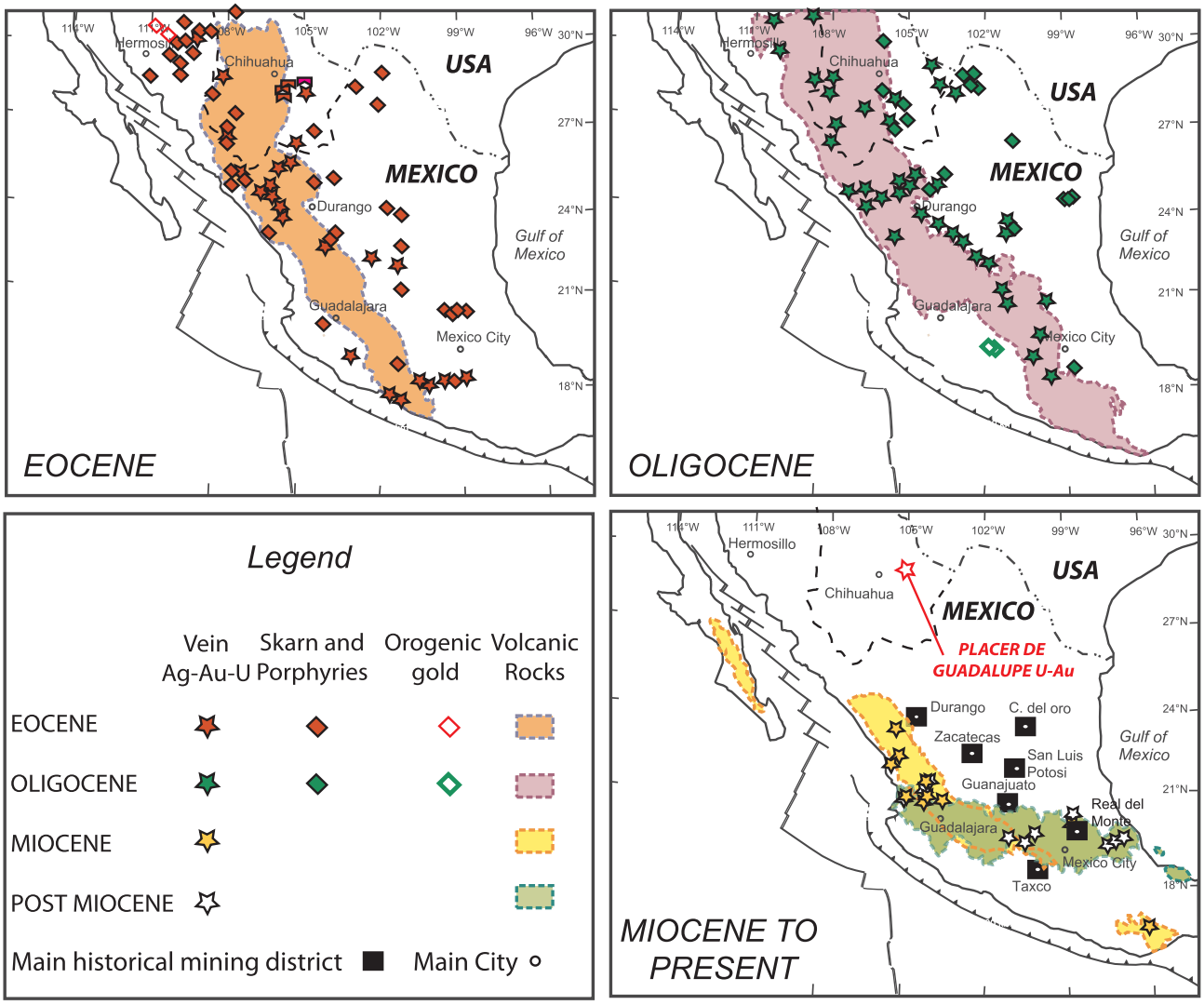

Fig. 1. Distribution of dated Mexican hydrothermal, skarn, porphyries and orogenic gold deposits from Eocene to recent, modified from Camprubi et al. (2013). Color shadows correspond to extensional volcanic rocks from the Eocene, Oligocene, and Miocene to recent, modified from Ferrari et al. (2012).

and Albinson, 2007; McLemore and North, 1984; Mc Lemore, 2011; Nieto-Samaniego et al., 2005; Camprubi, 2013). In Mexico, the chronological distribution of mineral deposits coincides with the distribution of the products of the three main volcanic pulses of the Sierra Madre Occidental, which are Eocene to early Miocene in age and record a broad migration from the northwest to the southeast, where the last ignimbrite flare-up occurred (Camprubí, 2013; Ferrari et al., 2005; McLemore and North, 1984; Mc Lemore, 2011; Ramos-Rosique A et al., 2011; Ramos-Rosique 2013; Fig. 1). The youngest and most fertile event, which outcrops in the northern and central regions of Mexico, ranges from 36 to 28 Ma in age and includes all of the largest Ag mining districts (Fig. 1). Although central Mexico is better known as a silver-bearing region (e.g., the Mexican Silver belt), it also contains many important gold and uranium resources, such as the La Paz Au-Cu skarn (Pinto-Linares et al., 2008), the Peñasquito Au deposit (Rocha-Rocha, 2016), and the Peña Blanca U deposit (George-Aniel et al., 1991; Angiboust et al., 2012). The central and northern regions of Mexico contain several deposits recording distinct styles of uranium mineralization, such as the volcanic-related type (Peña Blanca, San Marcos, Chihuahua; Goodell, 1981, George-Aniel et al., 1991; Reyes-Cortés et al., 2010, 2012; Angiboust et al., 2012), the roll-front type (La Coma, Nuevo Leon; Herrera-Monreal, 2011), placers and epithermal veins (Placer de Guadalupe; Chihuahua; Krieger, 1932) and the recently remobilized type (Sierra de Gomez, Chihuahua; Villarreal-Fuentes et al., 2016). Gold mineralization in Central Mexico can be classified as pluton associated deposits (i.e., porphyry or skarn) or epithermal vein deposits (Gilmer et al., 1988; Pinto-Linares et al., 2008; McLemore and North, 1984; Mc Lemore, 2011; Velador et al., 2010; Moncada et al., 2012; Mango et al., 2014; Camprubí, 2013). Epithermal vein mineralization is the most common style of Ag-Au deposits. The contents of Au/Ag metals can vary by several orders of magnitude within and between individual structures (Hayba et al., 1985; Sillitoe, 1993; Velador et al., 2010; Hall et al., 2014); for example, some structures only record Au mineralization, such as those in the Placer de Guadalupe district (Gonzales Reyna, 1946), the Fresnillo district (Velador et al., 2010) and the Zacualpan district (Hall et al., 2014), among others. This variation is generally interpreted to result from the circulation of lateral fluids and proximity to the source of the metals (Hynes, 1999; Camprubi and Albinson, 2007; Camprubi, 2013; Velador et al., 2010; Moncada et al., 2012; Mango et al., 2014). Velador et al. (2010) showed that the ages of the Au-dominant (Saucito mine) and Ag-dominant (i.e., the Santo Niño vein) structures within the Fresnillo district are comparable ca. 29 Ma, and suggested that the circulation of lateral fluids could explain the differences in mineralization between these districts. Additionally, Hall et al. (2014) and Enriquez and Rivera, 2001 suggested that variations in the silver/gold ratios in the Zaculpan and Tayoltita districts are controlled by their proximity to felsic intrusions.

The Au-U Placer de Guadalupe deposit in the state of Chihuahua is a

significant feature of Mexican geology. Its discovery initiated the last gold rush in Mexico at the end of the nineteenth century. It was also one of the first mineral deposits dated in Mexico, when direct dating of a clean uraninite crystal by Wells (1930) yielded an age of ca. 36 Ma. Krieger (1932) and Gonzales Reyna (1946) each developed monogenetic U-Au hydrothermal vein metallogenic models related to the emplacement of undated porphyry dykes (that were actually Permian in age; Villarreal et al., 2014), or blind Oligocene volcanism, respectively. Within the Ag/Au mining district, the Placer de Guadalupe Au-U district comprises various sets of mineralizing structures with U/Au ratios varying from pure gold to pure U (see below). The Au-U Placer de Guadalupe district represent a unique association of metals in Mexico; such deposits are not common worldwide, but are generally interpreted to represent the products of a series of various metallogenic events (i.e., Central French massif: Cuney et al., 1990; Boiron et al., 2003; Witwatersrand: Phillips and Powell, 2015). Despite the scientific and economic importance of the Guadalupe-Plomosas uplift, previous studies of this particular Mexican geological feature are scarce, and scientific discussion regarding the description and genesis of the Au-U Placer de Guadalupe deposits remains open today.

In this paper, we present a new geological description and geochemical characterization of the Au-U Placer de Guadalupe deposit. Our results provide key data that highlight, for the first time, the occurrence of telescoped Eocene uranium and Miocene Au metallogenic events in the state of Chihuahua and provide a better understanding of the formation of this complex Au-U epithermal deposit within the context of a coherent regional geodynamic evolution.

2. Regional geological setting

The Placer de Guadalupe district is a tectonic horst located in the physiographic Chihuahua basin-and-range style region (Hennings, 1994; Haenggi, 2002; Fig. 2), which is characterized by a succession of ranges and endorheic basins. The crystalline basement is Grenvillian to early Jurassic in age (Mauger et al., 1983; Iriondo et al., 2004; Villarreal et al., 2014). The Grenvillian basement is composed of *meta*-igneous rocks (1080–1333 Ma, Blount, 1993) and undated amphibolite intruded by trondhjemite, tonalite and granite (Mauger et al., 1983). During the Paleozoic, the Chihuahua region formed the southern passive margin of the continent Laurentia. Between the Triassic and the Lower Jurassic, the Pedregosa back-arc basin was a dominant paleostructure filled by carbonate to arenaceous formations (Stern and Dickinson, 2010; Averil and Miller, 2013). During the Mesozoic, this structure developed into to the proto-Chihuahua Basin, which was bounded to the west by the Aldama platform and to the east by the Diablo Platform. This major paleostructure controlled the structural and sedimentary evolution of central Chihuahua until the present, and is highlighted in outcrop as the Chihuahua central graben (Stern and Dickinson, 2010; Villarreal et al., 2014; Fig. 2). It contains a Mesozoic limestone succession that lies on top of an early Jurassic evaporite (Hennings, 1994; Haenggi, 2001). This stratigraphic succession was progressively deformed by various events of the Cordilleran orogeny (i.e., Sonoma, Nevadan, and Laramide; Drewes, 1981; Ingersoll and Schweicker, 1986; Domeier and Torsvik, 2014; Villarreal et al., 2014). The mountains in this region, which are composed of early Triassic to Late Cretaceous sedimentary rocks folded during the Laramide orogeny, are covered by a series of undeformed Cenozoic volcanic sequences (Hennings, 1994; Haenggi, 2001; Villarreal et al., 2014). Cenozoic volcanism in the area has been dated to between 46 Ma and 23 Ma (Cameron et al., 1989, and references therein; McDowell et al., 1997; Ferrari et al., 2005; Oviedo-Patron et al., 2010; Mahar et al., 2016). These volcanic deposits have been interpreted to comprise a member of the Sierra Madre Occidental (SMOc) volcanic province (Figs. 1, 2; Megaw et al., 1988; McDowell et al., 1997; Ferrari et al., 2005; Oviedo-Patron et al., 2010). The first Eocene volcanic flows rest unconformably atop Mesozoic rocks and have a low dip angle (Ferrari et al., 2005; Oviedo-Patron et al., 2010). The emplacement of these flows was coeval with extensional events that occurred during the Eocene and Miocene (Ferrari et al., 2005). The Eocene volcanic rocks of the SMOc (ca. 36 Ma; ^{40}Ar-^{39}Ar; Nandigam et al., 2009) are crosscut and covered by undated carbonatitic dykes and flows (Nandigam et al., 2009). During the Late Oligocene, extension moved north to the Rio Grande Valley and the Trans Pecos area (Price et al., 1987; Humphreys, 1995; Fig. 2). Between 25 and 10 Ma, the initiation of the Rio Grande rift extensional period produced bimodal volcanism (Price et al., 1987; Ricketts et al., 2015; Mahar et al., 2016). Ignimbrite flows and an alkalic basalt dike swarm were extruded along NNW-trending structures (Price et al., 1987; Mahar et al., 2016). From the Pliocene to the present, Cenozoic volcanic flows and detrital materials filled the Rio Grande basins (Bartolino, 1992; Haenggi, 2001). Finally, the Camargo volcanic field, which is Plio-Pleistocene in age (4.7–0.09 Ma; Aranda-Gomez et al., 2003; Fig. 2), lies midway between the Sierra Madre Occidental and the Trans-Pecos region of Texas (Fig. 2). This has been characterized as an intraplate mafic alkalic volcanic event that was strongly controlled by northwest-striking normal faults (Fig. 2; Aranda-Gomez et al., 2003).

3. History and geological setting of the placer de Guadalupe Au-U district

The Placer de Guadalupe Au-U district was discovered in 1867, when gold and uranium nuggets were found in sediments of the Plomosas river. It is considered to represent one of the first sites of uranium exploitation on the North American continent and was described in the mid-1900s as a hydrothermal gold-uranium mineral deposit (Krieger, 1932; González Reyna, 1946, 1956). Regional and local exploration, characterization, and preindustrial production were initiated in the early 1900s by the La Virgen Company (in the La Virgen U mine), Mexican Gold Dredging and the Mexican Goldfield (which mined Au in placer deposits). This 'gold fever' began to wane from 1915 to 1920 with the Mexican Revolution, the First World War and finally the end of superficial 'sweet spots'. The Au-placers and Au-U hydrothermal veins were sporadically mined for gold by "gambusinos" until the present without reaching an industrial level, mainly due to the restrictive Mexican Mining Law regarding strategic uranium reserves. Although no reliable production data or estimates of U and Au reserves are available, González-Reyna (1956) reported that, in 1911, the production in the La Virgen mine reached 0.2 tonnes of gold per month with a mean grade of 30 g/t. Gonzalez Reyna (1946) further estimated that gold production from 1875 to 1954 comprised 20 tonnes of Au from placer deposits and 0.65 tonnes of Au from vein deposits. The gold reserves estimated (and surely overestimated) in 1954 for PdG district were 22.5 thousand tonnes (Gonzalez Reyna (1946)). Historically, decimeter-scale gold nuggets have been found in river sediments. One of the remarkable characteristics of the Placer de Guadalupe deposit is the purity of its gold (99.99%; Gonzalez Reyna (1946)).

Within a regional geological context, the Placer de Guadalupe mining district features some specific geological characteristics. The Placer de Guadalupe ranges are formed by a WNW-trending tectonic stack comprising a large variety of magmatic and sedimentary formations (De Cserna et al., 1968; Torres et al., 1999; Villarreal et al., 2014; Fig. 3). The main thrust faults record a southwestward transport direction, opposite of the Laramide deformation structures (Bridges, 1962; Hennings, 1994; Goodell and Feinstein, 2008; Fig. 3). The basement outcrop at the Cerro Carrizalillo contains a chronological succession of undated amphibolite intruded by trondhjemite, tonalite and granite. Mosher (1998) correlated this outcrop with Grenvillian rocks in central Texas. The Paleozoic series comprises a succession of calcareous and arenaceous units known as the El Paso, Cable Canyon, Montoya, Percha, Escabrosa Paradise and Horquilla formations. All of these formations contain fauna from the mid-Ordovician to the Pennsylvanian (Bridges, 1962). The Middle Jurassic Upper Plomosas Formation contains shale and siliciclastic to conglomerate rock (ca.

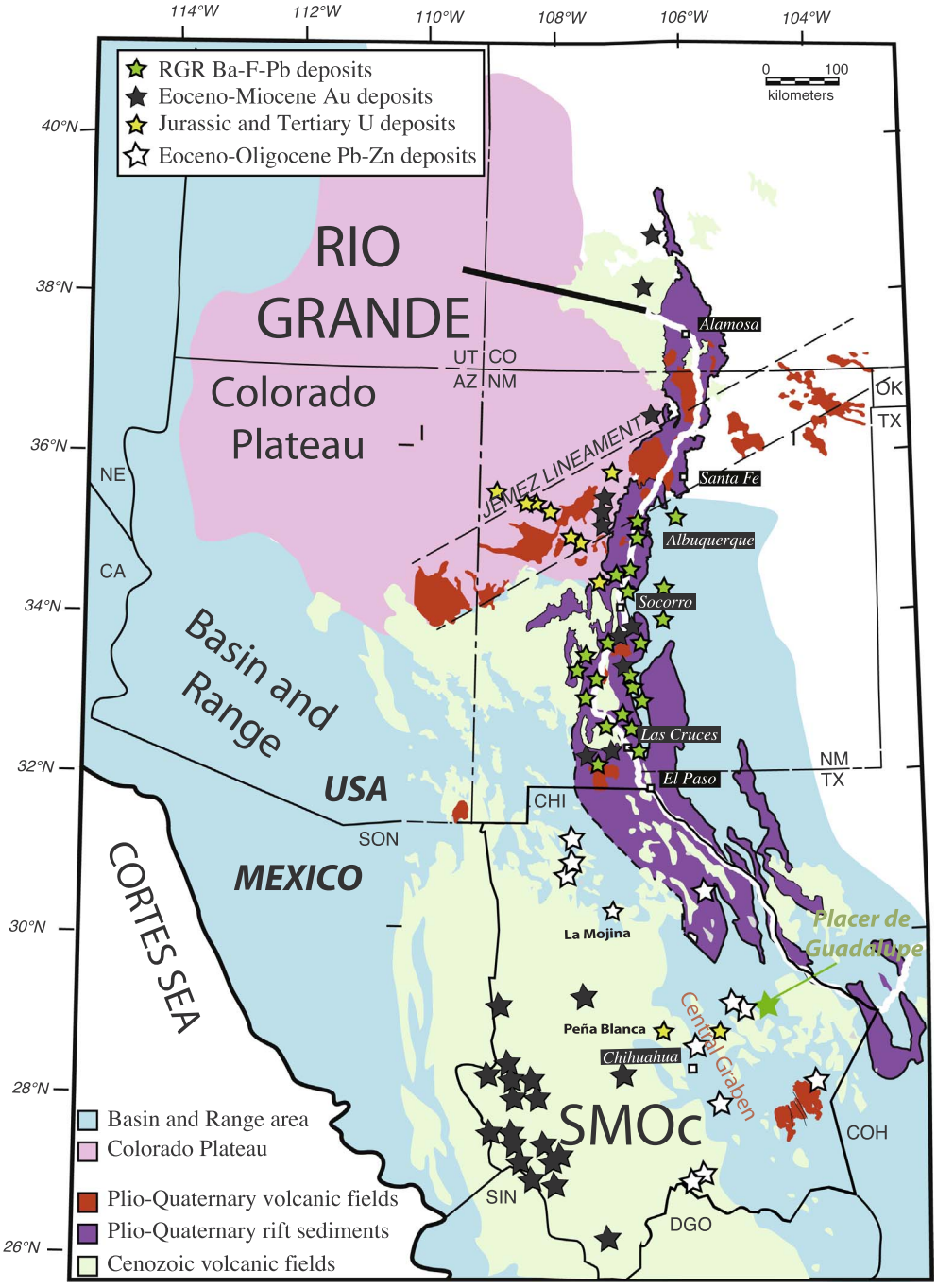

Fig. 2. Main geological provinces in NW Mexico and SW USA. Locations of the Rio Grande rift basins and its precursory and associated volcanic fields are modified from Hudson and Grauch (2013). The Cenozoic volcanism shape is modified from Ferrari et al. (2005); shapes of the Basin and Range and Colorado Plateau are modified from Baldridge et al. (1984). SON: Sonora, CHI: Chihuahua, TX: Texas, OK: Oklahoma, UT: Utah, CO: Colorado, AZ: Arizona, CA: California, NM: New Mexico, COH: Coahuila, DGO: Durango, SIN: Sinaloa.

168 Ma, U-Pb on single zircons; Villarreal et al., 2014) with interstratified volcanic flows (ca. 171 Ma, U-Pb on single zircons; Villarreal et al. (2014); Fig. 3) and limestone. Finally, the La Casita Formation, which is Kimmeridgian in age (King and Adkins, 1946), is composed of sandstone intercalations in lutite. The intrusive bodies mapped in the area are Late Triassic granite tectonic flakes (ca. 209 Ma, U-Pb on single zircons; Villarreal et al. (2014); Fig. 3), rhyolitic dykes and subaerial porphyry stocks that are likely Paleogene in age (Fig. 3).

4. Sampling and analytical techniques

4.1. Sample strategy

Calcite and gold-uraninite separates of different habits and colors deposited throughout the main paragenetic stages were collected from the La Virgen (LV) and Puerto del Aire (PdA) abandoned mine galleries. Mineralization samples were identified by using a Geiger detector in the abandoned working front.

4.2. Petrography

Mineralogy was documented through field observations and petrographic and SEM analyses. Mineral phases were identified using an scanning electron microscopy with X-ray microanalysis at the Laboratorio de Geofluidos in the Centro de Geociencias, Universidad Nacional Autónoma de México, Querétaro, Mexico. Host rocks and calcite cements were studied using a Reliotron® cold cathode cathodoluminescence (CL) device attached to an Olympus SZ-X binocular microscope and a Qimage Micropublisher 5 Mp digital camera with a Peltier cooled charge couple device (CCD). The electron beam had an

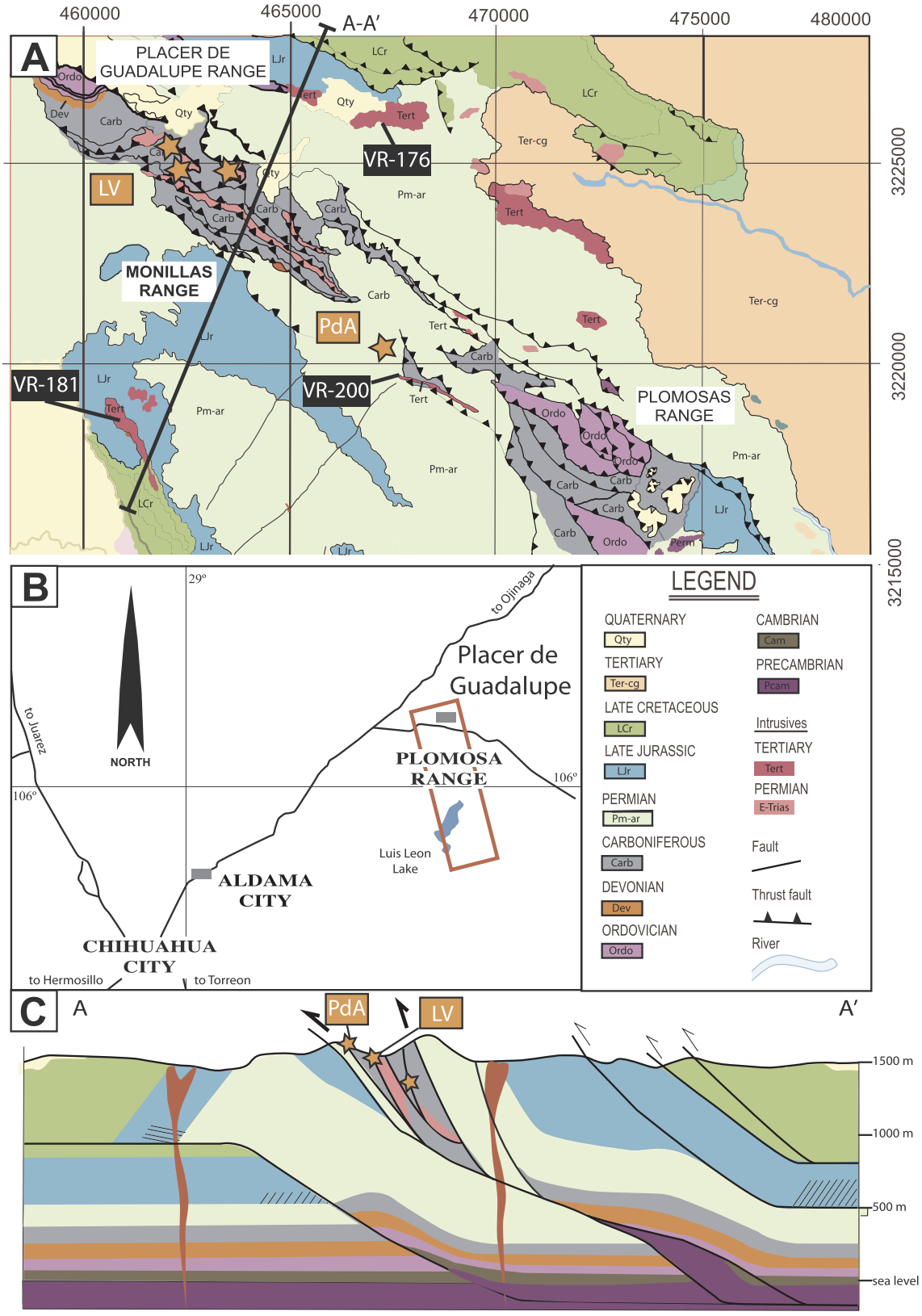

Fig. 3. A) Simplified geologic map of the study area. B) Regional localization map. C) Simplified geological cross-section of the Au mineralized district. Locations of volcanic samples are indicated by black squares. Studied mines are highlighted by orange stars.

acceleration voltage of 15 kV and a probe current of 500 μA. CL emission was enhanced by observing quartz samples on a copper plate previously cooled by immersion in liquid nitrogen. Thin sections were examined using a petrographic Olympus® BX-50 optical microscope with a Qimaging Micropublisher 5 Mp digital camera equipped with a Peltier-cooled CCD.

4.3. U-Pb geochronology

Three rock samples were collected from the intrusive bodies of interest (Fig. 3). These samples were crushed, powdered, and sieved (200–50 mesh). Heavy mineral fractions were obtained by density preconcentration with heavy liquids (methylene iodide). The non-magnetic fraction was separated using a Frantz isodynamic magnet. Final zircon separates were hand-picked under a binocular microscope and mounted in epoxy resin together with a standard (NIST), and subsequently polished. Laser ablation target points were selected on cathodoluminescence images in order to identify zircon cores and overgrowth zones.

Zircon samples were analyzed at the laser ablation facility at the Laboratorio de Estudios Isotópicos (LEI), Centro de Geociencias, UNAM. The instrument consisted of a Resonetics excimer laser ablation workstation (Solari et al., 2010) coupled with a Thermo XII_{Series} quadrupole ICPMS. The laser ablation workstation comprised a Coherent LPX 200, 193 nm excimer laser and an optical system equipped with a long working-distance lens with a 50–200 μm focus depth. The ablation cell was He-pressurized and capable of fast signal uptake and washout. Each analysis used a drill size of 34 μm and a drill depth of approximately 20–25 μm, producing a total ablated mass of ~70–80 ng during each analysis. Seventeen isotopes were scanned during each analysis. This made it possible to obtain quantitative measurements of the isotopes needed for U-Pb dating (i.e., lead, uranium and thorium), as well as detailed measurements of major and trace elements, such as Si, P, Ti, Zr and REEs, which can yield important information about the presence of microscopic inclusions in the zircons (e.g., monazite, apatite, or titanite) that can produce erroneous age results. For each analysis, 25 s of signal background were monitored, followed by 30 s of signal, in which the laser fired on the target with a frequency of 5 Hz and an energy density of ~8 J/cm^2. The remaining 25 s were used for washout and stage repositioning. A normal experiment involved the analysis of natural zircon standards and standard glasses. NIST standard glass analyses were used to recalculate U and Th concentrations in zircon. Repeated standard measurements were used for mass-bias correction, as well as for the calculation of down-hole and drift fractionations.

4.4. K-Ar geochronology

K-Ar analyses were performed on matrix samples from a rhyolite dyke at the Instituto de Geologia, UNAM. Samples were obtained by crushing with steel jaws, sieving, selecting the best fraction (300–400 μm), washing, separating the matrix glass by magnetic methods (using an Isodynamic Frantz separator), and performing minor manual grinding with a mortar and pestle. The K content of each sample was measured by X-ray fluorescence on 50 mg aliquots, using a specific regression for measuring K in K-Ar samples (Solé and Enrique, 2001). Analytical precision was > 2%. Samples weighing between 1 and 2 mg were degassed under high vacuum at ~150 °C for 12 h prior to analysis in order to reduce atmospheric contamination. Argon was extracted by total sample fusion using a 50W CO_2 laser defocused to 1–3 mm diameter. The evolved gases were mixed with a known amount of ^{38}Ar spike and purified with a cold finger immersed in liquid nitrogen and two SAES getters in a stainless-steel extraction line. Measurements were performed in static mode with an MM1200B mass spectrometer using electromagnetic peak switching controlled by a Hall probe. Analytical precision on ^{40}Ar and ^{38}Ar peak heights was > 0.2%, and that on ^{36}Ar was > 0.6%. These data were calibrated with internal standards and the international biotite reference materials LP-6 and HD-B1. All ages were calculated using the constants recommended by Steiger and Jager, 1977. A detailed description of the procedure and its calculations is given in Solé (2009).

4.5. U Mineralization geochronology

Uranium grains were collected from the Puerto del Aire Au-U vein mine (Fig. 3). The selected mineral separates were handpicked under a binocular microscope to ensure that the resulting samples were clean and pure. All selected grains are subhedral to euhedral. In situ U/Pb dating of uraninite was performed on polished thin sections by laser ablation–inductively coupled plasma–multi collector mass spectrometry (LA-MC-ICP-MS) at Queen's University, Canada. The laser used was a Mercantek LUV-213 Laser Ablation System with a frequency quintupled Nd-YAG (213 nm) used in raster mode. The laser conditions included a laser power output of 40–45% (< 1 mJ/cm^2), pulses of 50 ms with a repetition rate of 2 Hz, and a spot size of 25–35 μm. A Thermo Finnigan Neptune MC-ICP-MS instrument, equipped with 9 Faraday cups and 1011 Ω amplifiers for each, was also used.

4.6. Analysis of fluid inclusions

Double-polished wafers were obtained from Au-U-mineralized samples from the Puerto del Aire and La Virgen Mines. Wafers were inspected under a petrographic Olympus® BX-50 optical microscope with a Qimaging Micropublisher 5 Mp digital camera equipped with a Peltier-cooled CCD. Microthermometric data were acquired on a Linkam THMSG-600 stage attached to an Olympus® BX-50 petrographic microscope equipped with ultralong working distance objectives at the Crustal Fluids Laboratory of the Centro de Geociencias at UNAM in Querétaro. This stage facilitated the observation of fluid inclusion phase transitions from −193 to +600 °C with an accuracy of ± 0.1 °C. The stage was calibrated using Synflinc® synthetic fluid inclusions and ultrapure chemicals with a fixed melting point.

Raman microspectroscopy was used to determine the gas contents of these aqueous inclusions. The Raman spectrometer used in the CINESTAV-Conacyt laboratory was a High Resolution Labram type (Dilor), equipped with a Notch filter and a grating (1800 grooves per mm) to make it luminous. The detector was a CCD cooled at −30 °C, and the exciting radiation was provided by an Ar^+ laser (Type 2020, Spectraphysics) at 514.5 nm. The spectral resolution was approximately 2 cm^{-1}. The accumulation time, laser power and confocal aperture were modified for each inclusion measurement to obtain an optimum signal-to-noise ratio.

4.7. C-O isotopic analysis

Host rock limestone and vein cement calcites were sampled from the La Virgen and Puerto del Aire mines (Figs. 3 and 4). The selected mineral separates were handpicked under a binocular microscope to ensure that analyzed samples were clean and pure. Calcite cements were analyzed for their carbon and oxygen isotopic compositions using the CO_2 extraction method of McCrea (1950). Up to 15 mg of each sample was reacted with H_3PO_4 at 50 °C, and the collected CO_2 was analyzed in a Finnigan MAT Delta S thermal ionization mass spectrometer at the Serveis Científico-Tècnics of the Universitat de Barcelona. Reproducibility of the analyses of both isotopes was better than ± 0.1 per mil. C—O data are reported as per mil relative to VPDB. Data are grouped according to their paragenetic stage, from oldest to most recent (Fig. 7).

4.8. REE and trace element compositions

Crushed and powdered calcite cement and host rock samples were sent to be analyzed in the Actlabs, Canada commercial facilities. Each 0.25 g sample was digested with four acids, beginning with hydrofluoric acid, followed by a mixture of nitric and perchloric acids, and heated using precise programmer-controlled heating in several ramping and holding cycles to take the samples to dryness. After dryness was attained, samples were brought back into solution using hydrochloric and nitric acids. Total digestion may not have been attained if resistive

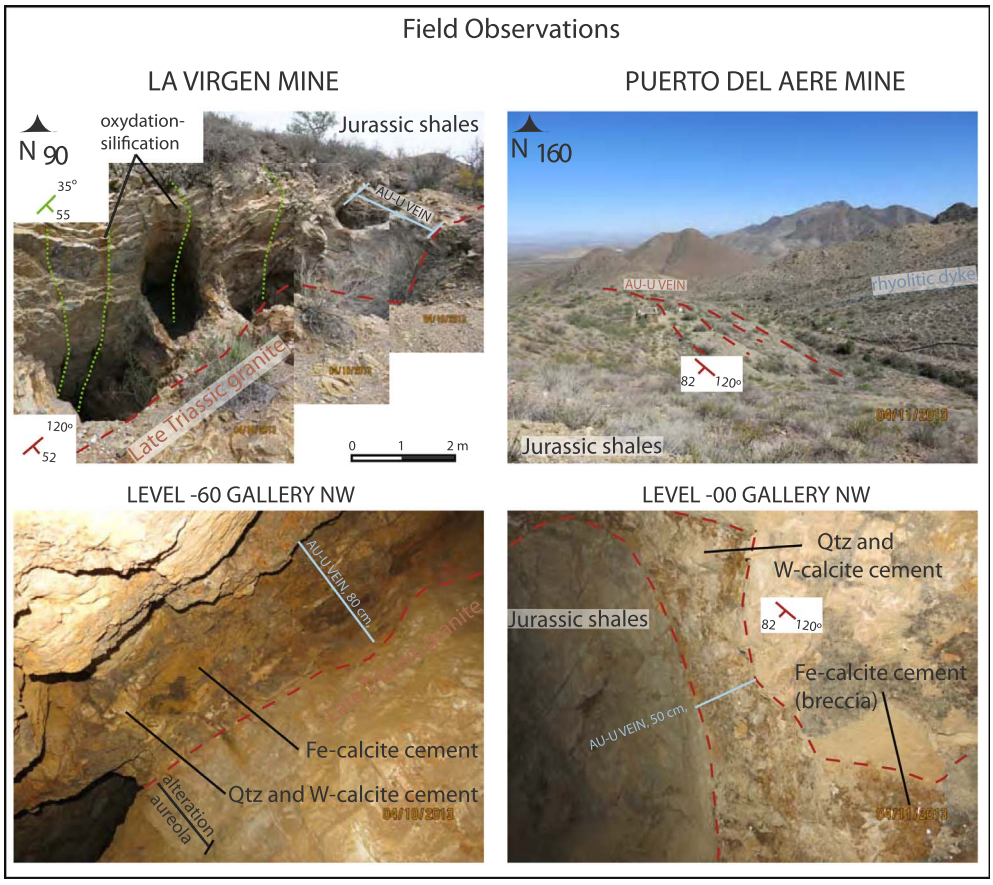

Fig. 4. Geological panorama and underground photography from the La Virgen and Puerto del Aire mines. Photographs highlight the structural control of the mineralized vein, the relation between Fe-calcite and silica and White calcite cement, and the limited development of alteration halos.

minerals were present. The elements of As, Sb and Cr may have been partially volatilized. An in-lab standard (traceable to certified reference materials) or certified reference materials were used for quality control. Digested samples were diluted and analyzed using a Perkin Elmer Sciex ELAN 9000 ICP/MS. One blank was run for every 40 samples, and an in-house control was run every 20 samples. Digested standards were run every 80 samples. After every 15 samples, a digestion duplicate was analyzed. The instrument was recalibrated every 80 samples.

5. Analytical results

5.1. New description of the Placer de Guadalupe Au-U district

The Placer de Guadalupe district is characterized by Au-U veins and Au-placers distributed in an area that is 30 km long and 3–5 km wide. In the northern and central parts of the Placer de Guadalupe district (which contains the La Virgen (LV), San Blas and Bolaños mines; Figs. 3 and 4), mineralization is hosted within a thrust fault located between a Late Triassic granite tectonic blade (ca. 209 Ma; Villarreal et al. (2014)) and an Early Jurassic shale (ca. 168 Ma; Villarreal et al. (2014); Figs. 3 and 4). The Au-U veins have trends ranging from 70° to 120° and are subparallel to the main structure of the Monilla thrust. The dips of the veins vary from 50°E to 90°E. These veins are continuous for nearly 3 km and are recognized to be 200 m deep (Figs. 3 and 4), with thicknesses ranging from 0.2 to 4.0 m. In the contact between the granitic flake and the mineralizing vein/thrust, the granitic groundmass has been intensely altered to sericite and kaolinite. The intensity of this alteration decreases throughout the granite flake. Feldspar phenocryst relicts, which retain the outlines of the original phenocrysts, can be observed in the sericite zones; several meters away, feldspar crystals of orthoclase and albite can be identified (Villarreal et al., 2014). In a few cases, Au-U mineralization fills joints and diaclases in the Late Triassic granite tectonic blade (Figs. 3 and 4). The Early Jurassic shale and the Au-U mineralizing vein record evidence of partial cement dissolution, carbonate recrystallization and silicification aureoles. The silicification intensity appears to increase with increasing Au/U ratio. The extent of the aureole through the Early Jurassic shale is limited by the stratigraphic joints.

In the southern part of the Placer de Guadalupe district, locally referred to as the “Puerto del Aire mine” (PdA; Figs. 3 and 4), mineralization is hosted within a sequence of five subparallel veins, separated by 10–30 m, that form a horsetail structure within the Middle Jurassic Upper Plomosas sandstone formation. These veins are continuous for almost 1 km and are nearly 50 m deep (Figs. 3 and 4), with thicknesses ranging from 0.4 to 1.0 m. Mineralized structures are spatially close to an undated, post-Jurassic rhyolitic dyke (Figs. 3 and 4). The alteration halo within the Upper Plomosas sandstone formation at Puerto del Aire is notable for its iron oxide contents. Carbonate dissolution and silicification are pervasive in the vein structure and, as in the northern part of the district, seem to control the Au/U mineralization ratio.

5.2. Petrography of the Placer de Guadalupe Au-U mineralization

Re-examination of the spatial and temporal relationships between the uranium and gold mineralization and the country rock indicates four distinct successive events: (i) a discrete (Ce, La)-rich calcite cement event; (ii) Fe and U hydrothermal mineralization event; (iii) gold hydrothermal mineralization event; and (iv) supergene enrichment.

(i) *(Ce, La)-rich calcite cement event:* The (Ce, La)-rich calcite cement event is only identified under catodoluminescence and electronic microscopy (Figs. 5 and 7).

(ii) *Fe-calcite cement event:* Transition from (Ce, La)-rich calcite event to Fe-calcite cement is evidenced by corrosion front (Fig. 5). Fe-

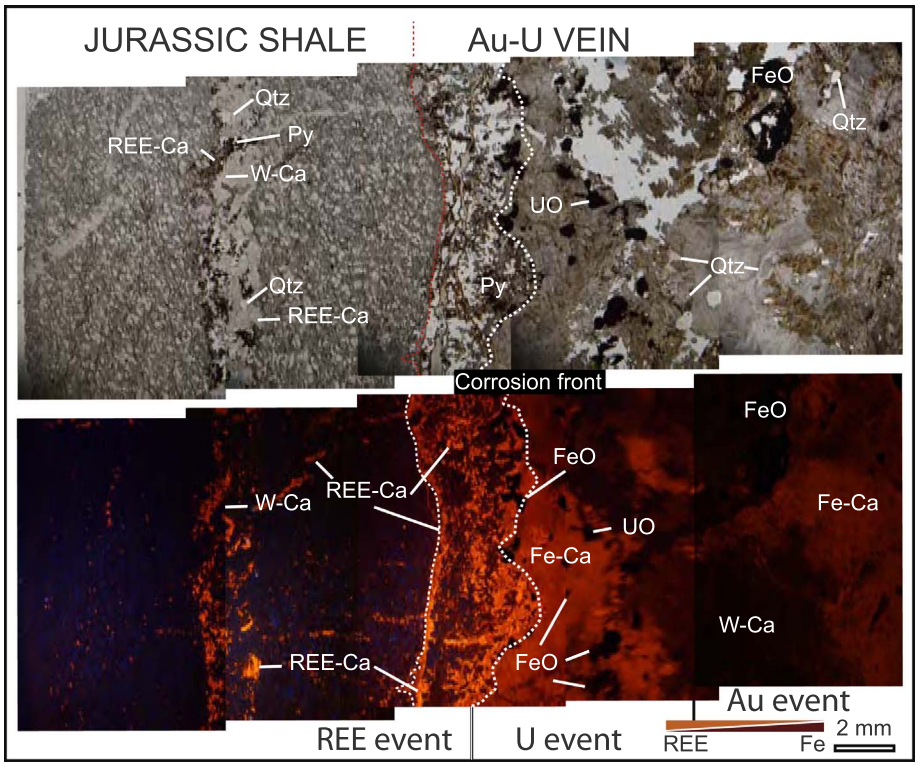

Fig. 5. Photomicrographs images taken under natural light and cathodoluminescence of thin section from the La Reina Au-U mineralized vein in the Puerto del Aire mine. (Ce, La)-rich calcites cement has a bright orange color under cathodoluminescence light. Petrographic evidence of dissolution is underlined in white doted line. Magnetite precipitation mark the beginning of the Fe calcite cement event. Abbreviations: W-Ca: white calcite; Fe-Ca: Fe stained calcite; FeO: iron oxide and oxidized pyrite; Qtz; quartz.

calcite are not siderite, but stained calcite with large amount of Fe-oxide within the clivage plane (Fig. 6). Magnetite precipitation mark the beginning of the Fe calcite cement event. Magnetite (specularite) is always prior to the uraninite occurrence. Magnetite and uraninite occur as crystals or aggregates of crystals up to a centimeter in size (Fig. 6). Uraninite crystals are cubic or octahedral in shape.

(iii) *Silica and white calcite cement event:* The host rock and Fe-calcite cement are fractured under overpressure hydraulic conditions, corroded and cemented by silica then white calcite. Mineralization is made of pyrite, chalcopyrite, and gold (Fig. 6). Pyrite and chalcopyrite are rare in la virgin structure and almost inexistent in the PdA vein. Gold mineralization occurs as native gold in the quartz and white calcite cements within the white calcite cleavage planes. Gold is also found within uraninite fractures in the Fe-calcites hydraulic breccia clast (Fig. 6).

(iv) Supergene alteration is intense, no sulphides remain in the first 50 m depth. The minerals observed include goethite, uranophane, free gold (with urophane in uraninite gost cavities), limonite, pyrolusite, and malachite (Figs. 5 and 6).

5.3. Geochronology

In Puerto del Aire, the undated post-Jurassic rhyolitic dyke (VR-200; Fig. 3) and two subaerial volcanic stocks (RV-176 and RV-181; Fig. 3) have different positions within the tectonic stack. They are the only geological elements without precise ages in the mining district's stratigraphic column. Thus, U-Pb dating of the volcanic rocks and uranium mineralization was performed to determine the chronological relationship between the volcanic emplacements and the Au and/or U mineralization events in the Placer de Guadalupe district.

5.3.1. U-Pb geochronology

Fifteen analyses of the VR-176 volcanic stock sample (Fig. 8) provide $^{206}Pb/^{207}Pb$ ages ranging from 35.4 ± 0.3 Ma to 37.5 ± 0.3 Ma. The weighted mean crystallization age (Ludwig, 2008) of zircons from the VR-176 intrusive sample is 37.0 ± 0.9 Ma. The two youngest ages form a distinct group that is more representative of a volcanic emplacement age of 35.7 ± 0.6 Ma ($n = 2$; MSWD of 0.1; Fig. 8, Supplementary Table 1).

Eighteen analyses performed on zircon crystals from the VR-181 volcanic stock (Fig. 8) yield $^{206}Pb/^{207}Pb$ ages ranging from 35.6 ± 1.3 Ma to 44.3 ± 0.4 Ma. One analysis was discarded due to its high sigma errors. Within the remaining seventeen concordant ages, sixteen analyses form a tight cluster with a distribution tail towards the younger ages. The weighted mean crystallization age (Ludwig, 2008) of zircons from the VR-181 intrusive sample is 37.8 ± 1.3 Ma. Nevertheless, the two youngest ages form a distinct group that is more representative of a volcanic emplacement weighted mean age (Ludwig, 2008) of 35.7 ± 0.8 Ma ($n = 2$; MSWD of 0.1; Fig. 8, Supplementary Table 2).

5.3.2. K-Ar geochronology

The low quantity of zircon crystals (most of which are inherited, dated at ca. 150 Ma; U-Pb on zircon monocrystal; these data are not discussed in this paper) within the Puerto del Aire post-Jurassic rhyolitic dyke (VR-200) makes it difficult to determine a coherent emplacement age using zircon dating. Therefore, the Puerto del Aire rhyolitic dyke was dated using K-Ar methodology. A thin section petrography study was performed to determine the mineralogy and the general preservation state of the sample in order to date it with the K-Ar method. The age determination was performed on matrix glass that was free of alterations. This K-Ar analysis yields a Bartonian age of 38.5 ± 0.5 Ma (7.79% K; 82.9% ^{40}Ar; 5.229 e^{-10} ^{40}Ar moles/g).

5.3.3. Puerto del Aire mine uraninite U-Pb geochronology

To determine the possible age of uraninite alteration caused by the gold hydrothermal event, we decided to specifically date only altered uraninite crystals crosscut by the gold sheet in a gold-rich vein from the Puerto del Aire mine. The disseminated uraninite grains sampled from the La Reina vein in the Puerto del Aire mineralizing area (Figs. 3 and 4) rarely exceed a millimeter in length. All analyzed grains are subhedral to euhedral, exhibit a metallic to submetallic luster, are fractured and are filled with gold sheets (Fig. 6).

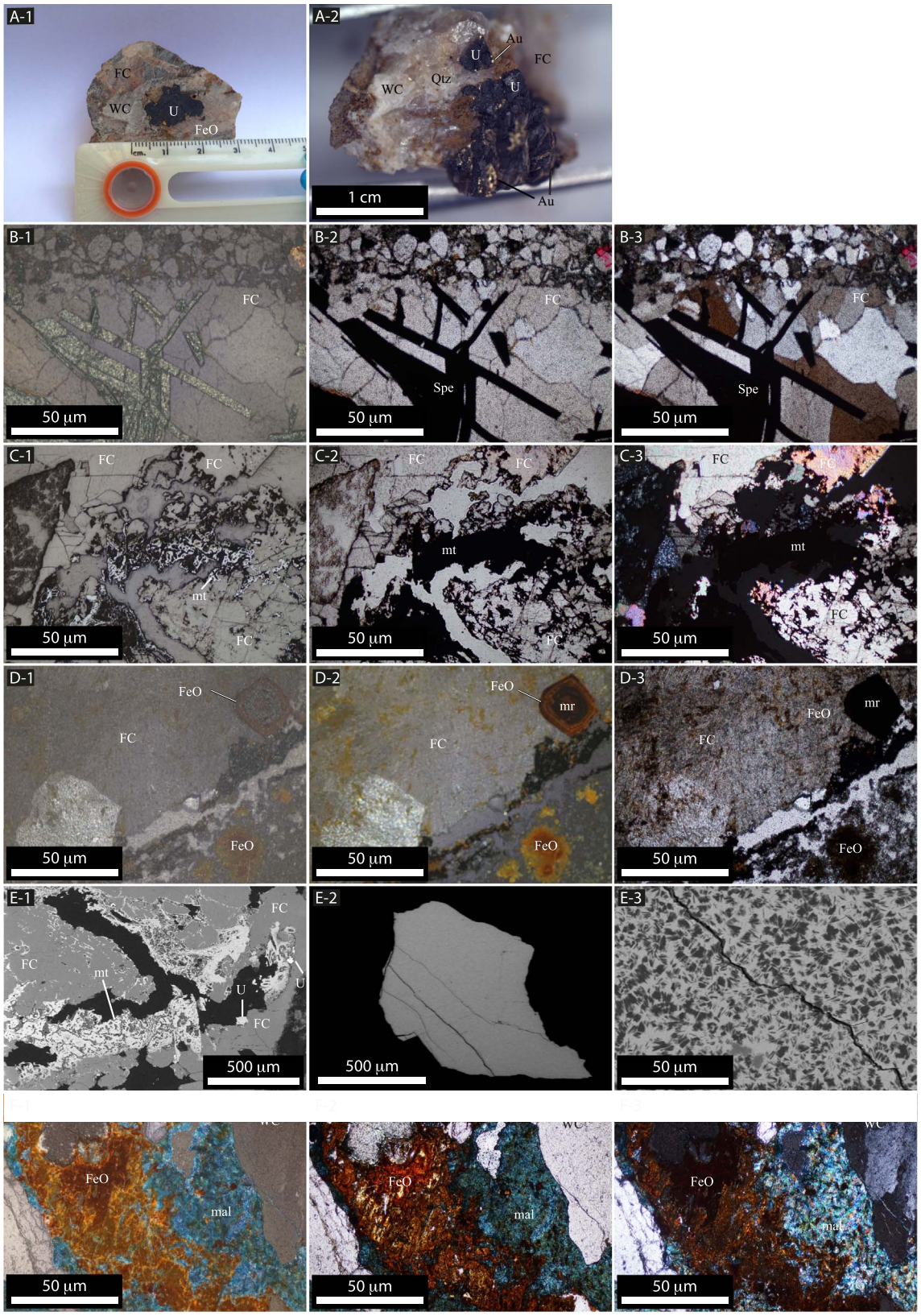

(caption on next page)

Twenty analyses were carried out on gold-uraninite grains from the Puerto del Aire mine, yielding $^{206}Pb/^{238}Pb$ ages ranging from 19.7 ± 0.6 Ma to 25.1 ± 1.5 Ma and $^{207}Pb/^{235}U$ ages ranging from 20.0 ± 1 Ma to 25.0 ± 1.9 Ma (Supplementary Table 2). All of the results are concordant ages that form a tight cluster (Fig. 8) indicating a weighted mean $^{207}Pb/^{206}Pb$ crystallization age of 20.9 ± 3.7 Ma (n = 20; MSWD of 0.1; Fig. 8).

Fig. 6. Photomicrographs image and BSE photographs of selected mineralization associations of the four distinct stages. (A-1, A-2) U-Au mineralized hand samples. (A-1): Uranium mineralization clast in white calcite cement. Clast is composed by uraninite, Fe-Oxide, limonite and Fe calcite cement. (A-2): Uranium and gold mineralization in PdG vein. See the gold sheet crosscuting the uraninite crystal and the quartz cementing the uraninite-Fe oxide and Fe calcite clast. (B-1, B-2, B-3) specularite in Fe-calcite (poorly stained) vein within the Middle Jurassic Upper Plomosas Formation (PdG): (B-1) photomicrograph with reflected light of thin section, (B-2) photomicrograph with plane polarized light, and (B-3) with crossed nicols. (C-1, B-2, B-3) Magnetite mineralization in Fe-calcite vein (PdG): (C-1) photomicrograph with reflected light of thin section, (C-2) photomicrograph with plane polarized light, and (C-3) with crossed nicols. (D-1, D-2, D-3) Supergene alteration of magnetite in Fe-calcite vein (PdG): (D-1) photomicrograph with reflected light of thin section, (D-2) photomicrograph with plane polarized light, and (D-3) with crossed nicols. (E-1, E-2, E-3) BSE photographs of uranium mineralization event: (E-1): Magnetite and uraninite crystal in Fe-calcite cement. (E-2) and (E-3; Enlargement of E-2) Uraninite altered to urofane. (F-1, F-2, F-3) Microphotographic images of supergene alteration of pyrite and chalcopyrite from gold event to Fe-oxide and malachite (La Virgen): (F-1) photomicrograph with reflected light of thin section, (F-2) photomicrograph with plane polarized light, and (F-3) with crossed nicols. Abbreviations: FC : Fe-calcite; WC : white-calcite; qtz quartz; mt : magnetite; hm hematite; mr marcasite; FeO : Fe-oxide; mal : malachite; mt : magnetite; U : uraninite; spe : specularite.

5.4. Fluid inclusions in the Au epithermal system

In the LV and PdA mines, the REE calcites and Fe-calcites are too dark to reliably observe. Since no suitable mineral hosts for fluid inclusions were formed during the U-hydrothermal event, microthermometric investigations were conducted only on primary fluid inclusions in quartz and white calcite stages from the gold mineralization in the Puerto del Aire (PdA) mine (southern district area) and the La Virgen (LV) mine (northern district area; Fig. 3). Microthermometric fluid inclusion results are presented in Fig. 9 and Supplementary Table 3.

Based on the petrographic and compositional features of these fluid inclusions at room temperature, three types of fluid inclusions can be identified: Type I: H_2O-CO_2-daughter mineral-bearing fluid inclusions; Type II: H_2O-saline fluid inclusions; Type III: CO_2-rich fluid inclusions. Type I polyphasic (Liquid-Vapor-Solid$_{1\text{-}2}$) primary fluid inclusions occur only in quartz and calcite stages from the PdA mine. All of these fluid inclusions are either found as isolated inclusions or in small clusters. This population of fluid inclusions yields very homogeneous volume ratios (Fig. 9). Typically, the fluid inclusions are negative crystals to ovoid in shape and are less than 60 μm in their maximum dimension with a cubic halite crystal. Few inclusions contain two solids, a cubic halite crystal and a calcite crystal, which can be identified by laser Raman analysis. Calcite crystals are interpreted to have been accidentally trapped, as no change in size (i.e., dissolution) is observed upon heating. The visual estimate of the liquid-to-vapor ratio is less than 0.6. All of the fluid inclusions studied in the PdA samples record CO_2 contents (as determined by microthermometry and confirmed by Raman microprobe analysis). Type II inclusions occur in the quartz and calcite stages of the LV mine (Fig. 9A). All of these fluid inclusions are primary and are found either as isolated inclusions, in small clusters in quartz or as pseudosecondary inclusions found along the calcite cleavage plane. In the quartz stage, type II fluid inclusions are spatially related to CO_2-bearing fluid inclusions (Type III; Fig. 9A). The type II fluid inclusions are biphasic, crystal negative to ovoid in shape and are less than 40 μm in the maximum dimension. The visual estimate of the liquid-to-vapor ratio is highly variable, and type II fluid inclusions generally record low CO_2 contents (as determined by Raman microprobe analyses). Type III fluid inclusions are CO_2-bearing fluid inclusions, which are only observed in the quartz stage of the LV mine (Fig. 9A). CO_2-bearing fluid inclusions are dominant in some quartz crystals, but are generally associated with Type II aqueous fluid inclusions in clusters. They are crystal negative to ovoid in shape and can be large in size, often > 200 μm in their maximum dimension.

In PdA, Type I polyphase fluid inclusions in quartz and calcite show complete homogenization (Th) by halite melting (Tm_{NaCl}) at temperatures ranging from 268 °C to 305 °C and 266.6 °C to 283 °C, respectively. Bubble shrinkage (Thv) into liquid, which occurs at temperatures ranging from 240 °C to 293 °C and 234 °C to 264 °C in quartz and calcite, respectively, always occurs at lower temperatures than halite melting (Fig. 9). As Tm_{NaCl} is systematically higher than Thv in the analyzed multiphasic fluid inclusions, the fluid's salinity cannot be determined using the ice melting temperature, but can instead be calculated as a function of the $Tm_{NaCl}/Th_{LV\text{-}L}$ relationship following the equations of Steele-MacInnis et al., 2012. The determined salinities remain very constant throughout the paragenetic sequence and on the scale of the PdA mine, yielding eq NaCl contents ranging from 35.9 to 38.9 wt% and 36.0 to 37.5 wt% for quartz and calcite, respectively. The Steele-MacInnis et al. (2012) equations also allow us to determine a range of

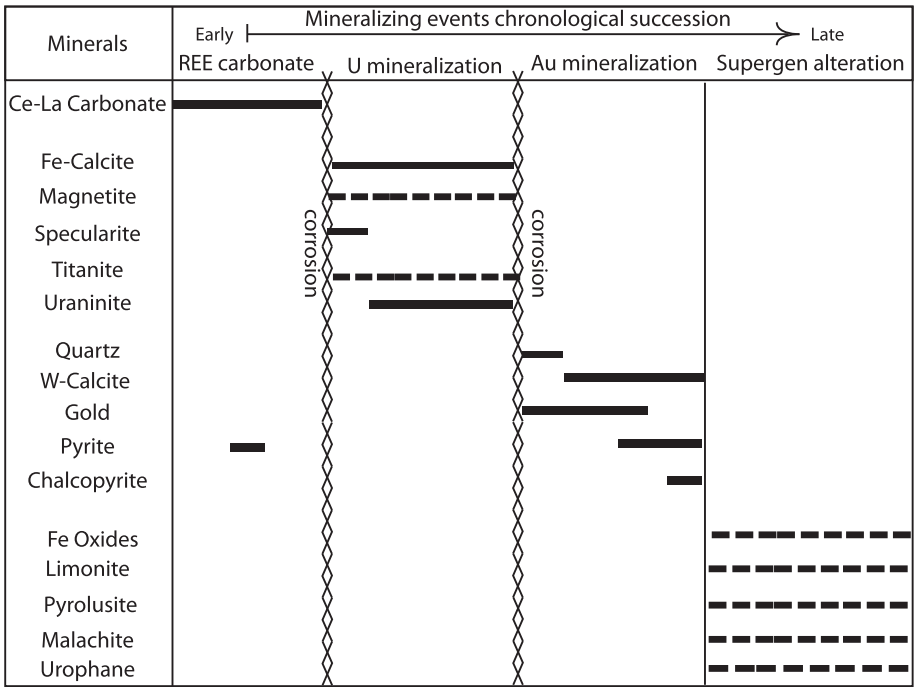

Fig. 7. Paragenetic sequence of the Puerto del Aire mine (PdA) and La Virgen vein U-Au deposits.

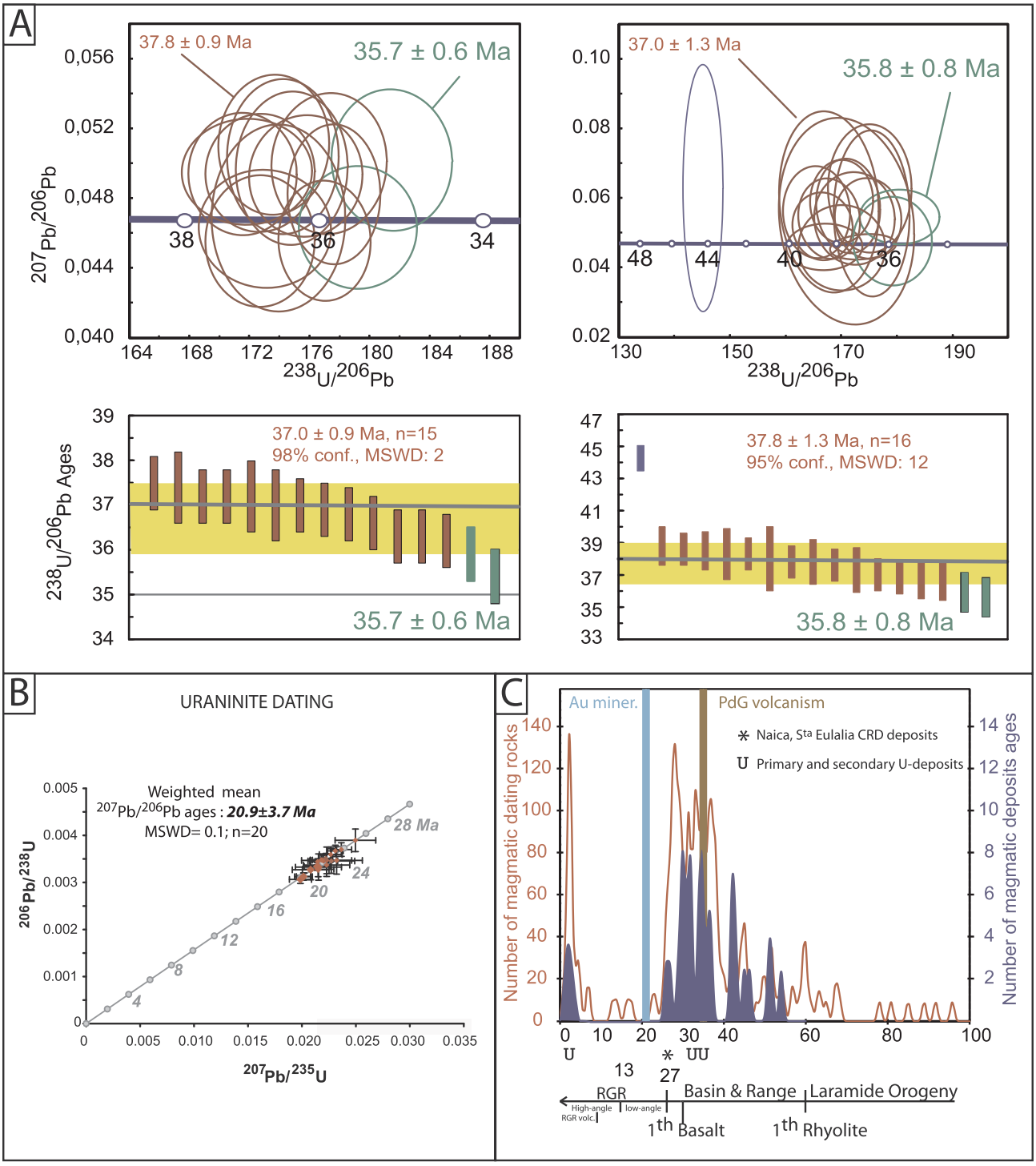

Fig. 8. A) Concordia diagrams of volcanic stock samples VR-176 and VR-181 dated by LA-ICPMS on zircon monocrystal. The diagrams, ages, and errors (1-sigma) were generated using the Isoplot 3.71 program (Ludwig, 2008). Ellipses are 1-sigma errors. Red ellipses correspond to the analyses used for the weighted mean age. Green ellipses correspond to the analyses used for the emplacement age. B) Concordia diagrams for the U-Pb isotopes of uraninite from the Au-U Placer de Guadalupe deposit. The diagrams, ages, and errors (1♦) were generated using the Isoplot 3.71 program (Ludwig, 2008). C) Histogram recording distribution of magmatic rocks (in red) and mineral deposits (in blue) within the Chihuahua state, Mexico.

multiphasic fluid inclusion trapping pore pressures; in the case of the PdA samples, these values range from 127 to 894 bars in quartz and from 414 to 795 bars in calcite (Fig. 9B).

In the LV samples, the type II biphase saline fluid inclusions in the quartz stage yield final ice melting temperatures ranging from −20.1 °C to −16.6 °C. In the calcite stage, the type II biphase saline fluid inclusions yield final ice melting temperatures ranging from −19.3 °C to −16.3 °C. Total homogenization occurs in the liquid phases of quartz and calcite at temperatures ranging from 218 °C to 252 °C and 217 to 232 °C, respectively (Fig. 9). The determined salinities remain very constant through the paragenetic sequence and on the scale of the LV mine, ranging from 20.0 to 22.5 wt% eq NaCl in quartz and 19.7 to 21.9 wt% eq NaCl in calcite (Steele-MacInnis et al. (2012) equations). The calculated trapping pore pressures are low, ranging from 19 to 34 bars in quartz and 22–34 bars in calcite (Fig. 9B). The melting temperatures of the LV type III CO_2-bearing fluid inclusions range from

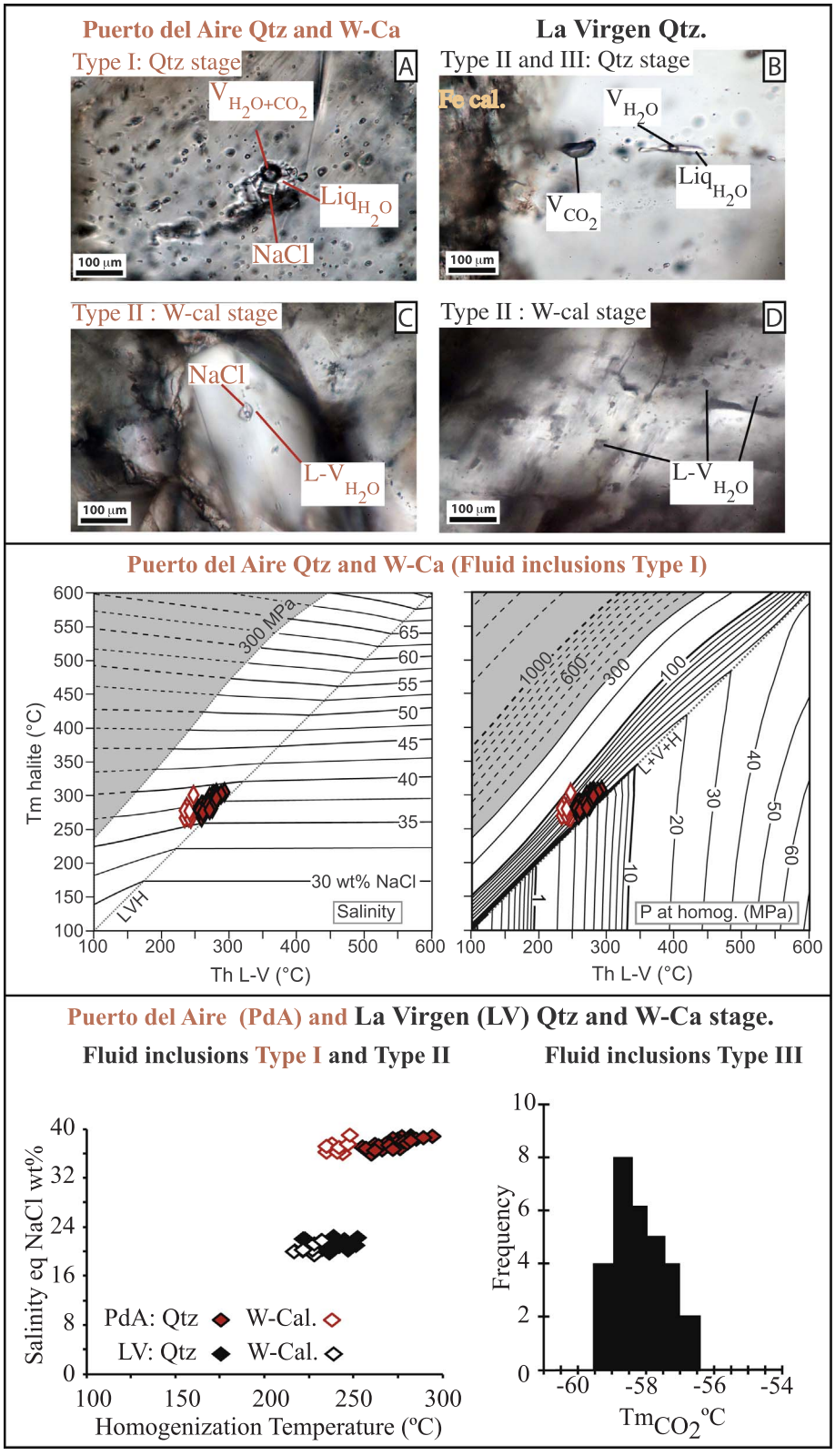

Fig. 9. A) Images of fluid inclusion types; B) temperature of homogenization vs. halite melting temperature plots for generations of type I fluid inclusions in quartz and white calcite cements (modified from Lefticariu et al., 2005); C) temperature of homogenization vs. salinity plots for generations of hydrothermal type I and II fluid inclusions in quartz and white calcite cements, as well as histogram recording the distribution of CO_2 melting temperatures of type III fluid inclusions in quartz.

−59.3 °C to −56.6 °C (Fig. 9C). These temperatures are slightly lower than the triple point for pure CO_2, suggesting the presence of a minor amount of H_2O (and possibly other gases, such as N_2 and CH_4), which is confirmed by laser Raman analyses.

On a diagram of salinity (S) versus homogenization temperature (Th) (Fig. 9C), the Type I and II fluid inclusions from PdA and LV are separated in two parallel, positively correlated lines. Both correlations record the same evolution from high-temperature quartz to lower-temperature calcite with homogeneous high salinity values, suggesting an adiabatic cooling process and/or low contributions of external fluids. While PdA is characterized by NaCl-oversaturated fluids, LV records CO_{2gas}- and liquid-bearing fluid inclusions with lower Th and salinity than PdA fluids, suggesting that they experienced different emplacement conditions.

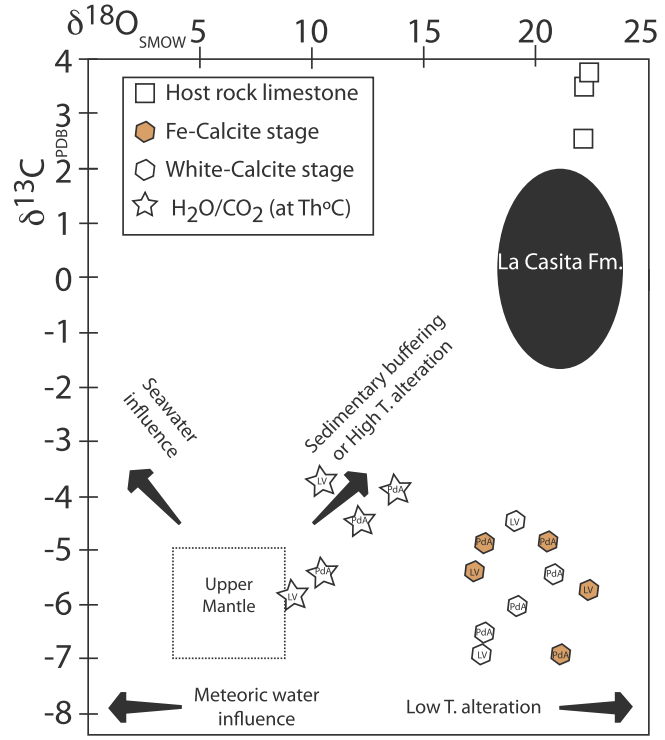

Fig. 10. Carbon and oxygen isotopic measurements of calcite from the Au-U Placer de Guadalupe deposits, shown together with the regional field of limestones (Kimmeridgian La Casita Formation, Taylor et al., 1967; Lefticariu et al., 2005) and typical mantle compositions (Ray et al., 1999).

5.5. C-O isotopic study of calcite cements from U- and Au-epithermal systems

To better trace the gold- and uranium-bearing fluid sources and the mineralization precipitation processes, we sampled and analyzed the host rock limestone, Fe-calcite and white calcite hydrothermal deposits from the Puerto del Aire (PdA) and La Virgen (LV) mineralization area (Fig. 10; Supplementary Table 4).

$\delta^{13}C_{PDB}$ and $\delta^{18}O_{SMOW}$ values measured in the host rock limestone record a restricted distribution of 2.58 ± 0.1‰ to 3.71 ± 0.1‰ and 22.04 ± 0.1‰ to 22.75 ± 0.1‰, respectively. $\delta^{13}C_{PDB}$ and $\delta^{18}O_{SMOW}$ values measured in Fe-calcite and white calcite samples are comparable (Fig. 10). The $\delta^{13}C_{PDB}$ and $\delta^{18}O_{SMOW}$ values of the PdA and LV Fe-calcite range from −4.8 ± 0.1‰ to −6.8 ± 0.1‰ and from 17.2 ± 0.1‰ to 22.3 ± 0.1‰, respectively. The $\delta^{13}C_{PDB}$ and $\delta^{18}O_{SMOW}$ values of the PdA and LV white calcite range from −4.4 ± 0.1‰ to −6.9 ± 0.1‰ and from 17.5 ± 0.1‰ to 20.7 ± 0.1‰, respectively (Fig. 10). The reported C–O isotopic compositions of the Fe and white calcite crystals are indistinguishable, suggest that the carbon is of magmatic origin (Cartigny et al., 1998), and indicate that the fractionation of oxygen has followed a trend of low-temperature alteration caused by magmatic–hydrothermal fluids (Fig. 10).

Assuming that the final homogenization temperature represents the minimum trapping temperature (see Section 5.4), it is then possible to calculate the isotopic composition of the parental fluids of the white calcite events using the isotopic fractionation equations of Zheng (1999) and Ohmoto and Rye (1979). The $\delta^{18}O_{fluid}$ and $\delta^{13}C_{CO2}$ isotopic values of the white calcite event at its mean final homogenization temperature (ca. 266 °C for PdA and 225 °C for LV; Fig. 10) range from 6.9 to 8.5‰ and −1.6 to −0.8‰, respectively. The $\delta^{18}O_{fluid}$ and $\delta^{13}C_{CO2}$ isotopic values of the white calcite parental fluid range from 9.1 to 13.8‰ (yielding a mean LV and PdA $\delta^{18}O_{fluid}$ value of 11.3‰) and from −5.3 to −3.6‰ (yielding a mean LV and PdA $\delta^{13}C_{CO2}$ value of −4.6‰), respectively (Fig. 10; Supplementary Table 4).

5.6. REE compositions of U- and Au-cements and magmatic and sedimentary host rocks

REE are valuable in identifying the sources of ore-forming materials and interaction processes, tracing the evolution of hydrothermal systems, and constraining the genesis of ore deposits (Henderson, 1984; Klinkhammer et al., 1994). REE concentrations and chondrite-normalized REY patterns of host rocks, Fe-calcite and white calcite hydrothermal events measured during this study, as well as additional data for Permian, Late-Jurassic and Eocene-Oligocene volcanic host rocks and carbonatite volcanic formations from previously reported studies are given in Figs. 11A and 10B and Supplementary Table 5.

Fe- and white calcites (FC and WC) are characterized by their relatively high total REE concentrations (ΣREE) ranging from 348.6 to 595.9 ppm and from 96.7 to 376.1 ppm, respectively. In addition to REE and Y (REYs), high field strength elements such as Ba, Nb, Ta, U, Th, and Zr are present in very small amounts, which are commonly close to the detection limit in Fe-calcite and an order of magnitude higher in concentration in white calcite. Fe- and white calcites can be distinguished by their REY patterns. In both cases, cerium anomalies are not present or are slightly negative (Ce/Ce^*_{WC} = 0.80–0.98; Ce/

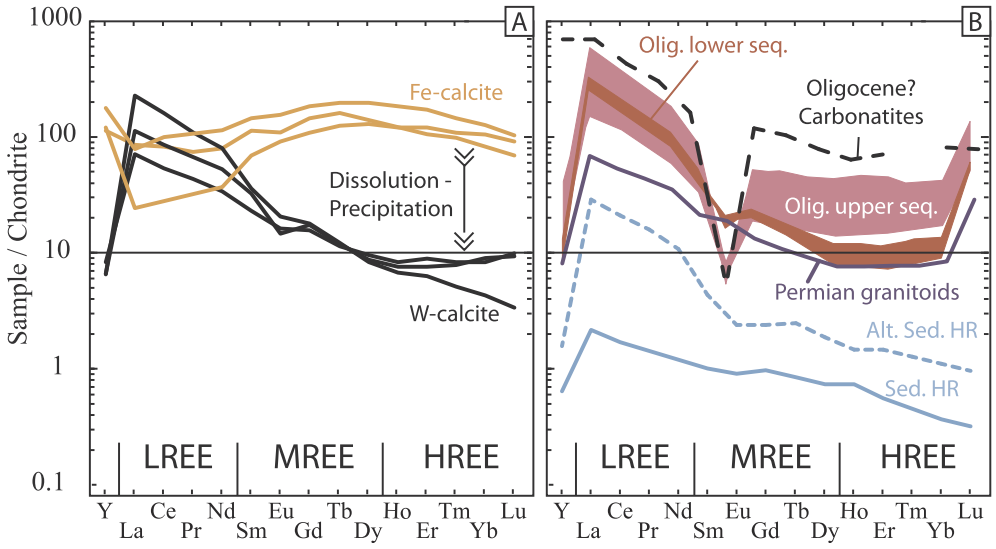

Fig. 11. Chondrite-normalized REE + Y patterns of magmatic and limestone host rock and calcite gangue from the Placer de Guadalupe Fe-U-Au deposit. All data are normalized by chondritic REE + Y values from Sun, 1989. Data points are connected by lines where possible, to show general patterns.

$Ce*_{FC}$ = 0.94–1.0). Additionally, europium anomalies are not present in Fe-calcite (Eu/Eu* = 0.87–1.40) and are slightly negative in white calcite (Eu/Eu* = 0.58–0.88; Fig. 11A). They record a narrow range of LREE (La, Ce, Pr, Nd) usually ranging between 10 and 100 times chondritic values, but vary greatly in their MREE (Sm, Eu, Gd, Tb, Dy, Y) and HREE (Ho, Er, Tm, Yb, Lu) concentrations, resulting in Fe- and white calcites plotting as two populations: Fe-calcites record flat MREE and HREE shapes (up to 100 times chondritic values) and white calcites record concave REY shapes (in which MREE and HREE are 10 times that of chondrite; Fig. 11A; Supplementary Table 5). The Y/Ho ratios in all mineralized samples range from 22.9 to 28.8.

As a comparison, we also present REE patterns of the main host rock and potential metal sources. Chondrite-normalized REY patterns of Eocene-Oligocene and Permian magmatic rocks display high REE concentrations with a moderate fractionation pattern (i.e., Y/Ho ratios ranging from 1.0 to 6.0). REE concentrations, fractionation intensity and europium anomalies increase over time from the Permian to the late Oligocene (Fig. 11B; Supplementary Table 5). The sedimentary formations record weak global fractionation, with REE profiles exhibiting a small negative slope and Y/Ho ratios ranging from 25.0 to 31.3, which are comparable to the calcite cements. Altered sedimentary formations display a general enrichment compared to the unaltered rocks; in particular, their LREE concentrations mimic the REY pattern of the Oligocene magmatic rocks (Fig. 11B; Supplementary Table 5).

6. Metallogenic model of the Placer de Guadalupe Au-U vein deposits

6.1. Timing of magmatism and U-Au mineralization events

Detailed geological field work shows a very strong structural control on metal deposition, exhibiting a wide range of Au/U ratios, ranging from U-only to Au-only deposits. U-Au mineralizations are hosted in thrust faults that have undergone multiple reactivations. Field observations, evidence for a dissolution front in the minerals' paragenesis and differences in their REE patterns suggest that at least two hydrothermal events, with different P-T-x conditions, occurred in the PdG district (Figs. 5–7). The textural and chemical evolution of the mineralizing systems cannot be explained by either water/rock interaction processes during various mineralization pulses in a long-lived hydrothermal system or by the telescoping of two different mineralization events (McIntosh, 2004; Tosdal et al., 2009; Kodera et al., 2005; Vidal et al., 2016). The very simple paragenetic succession does not seem to support the proposed single epithermal Au-U-vein event (Krieger 1932; Gonzalez Reyna, 1946), which is usually related to a polymetallic hydrothermal event (White and Hedenquist, 1990; Phillips and Powell, 2015). Wells (1930) previously obtained uraninite crystallization ages of ca. 36 Ma (U-Pb on unaltered uraninite population, La Virgen U-vein; Fig. 8). This mineralization age is comparable (within the margin of error) to the ages determined more recently from the Peña Blanca (32 ± 8 Ma, Fayek et al., 2006; Angiboust et al., 2012; Fig. 8) and San Carlos U-bearing volcanic deposits (Reyes-Cortés et al., 2010; Fig. 8). This suggests that regional U-mineralizing pulses with various mineralizing styles produced the vein- and volcanic-related type deposits. The unaltered uraninite population dated from the La Virgen U-vein (Wells, 1930) and the gold-cemented uraninites analyzed from the Puerto del Aire Au-U vein are comparable in their paragenetic position and are thus assumed to have precipitated from the same mineralizing epithermal event at 36–32 Ma (Wells, 1930; Fayek et al., 2006).

The gold-cemented uraninite from the Puerto del Aire Au-U vein yields a U-Pb age of ca. 21 Ma, which is almost 15 Ma younger than the measured age of the unaltered uraninite (Fig. 8). Fluids and/or thermal events affecting uraninite after its original formation may result in the complete or partial resetting of U-Pb systematics (Fayek and Kyser, 1997; Finch and Murakami, 1999). The uraninite has the ability to be reset and/or to dissolve and precipitate a secondary uranium mineral (Fayek and Kyser, 1997). This Miocene age thus does not represent the uraninite's crystallization age but instead the date of the last alteration event affecting the uraninite, which in this case, is the mineralizing event of gold cementing the uraninite fracture. U-Pb geochronology results confirm petrographic evidence of the occurrence of two distinct U and Au mineralizing events, which are Late Eocene and Early Miocene in age, respectively.

The U-Pb and K-Ar emplacement ages obtained from the dated volcanic rocks yield a tight range of emplacement ages from ca. 38.5 to ca. 35.7 Ma (Fig. 8). These intrusions are comparable in their stratigraphic position and ages to the Meza and carbonatite volcanic formations (Alba and Chavez, 1974; McDowell and Maugher, 1994). The overlapping ages of the volcanic intrusions (ca. 38.5–ca. 35.7 Ma) and the U-mineralization event (ca. 36 Ma) within the Placer de Guadalupe U district strongly indicate that these intrusions are a potential source of metals and heat (Fig. 8). The second volcanic sequence of the SMOc is characterized by its REE and volatile enrichment, with uranium content ranging from 3 to 15 ppm and from 2 to 637 ppm in the carbonatite volcanic formations (ca. 38 Ma to ca. 34 Ma; Cameron et al. (1989); McDowell and Mauger (1994); Orozco-Esquivel et al. (2002); Oviedo-Patron et al. (2010); Nandigam et al. (2009); Iriondo et al. (2004)). Therefore, the late Eocene volcanic intrusions represent an efficient thermal and potential metal source for the generation of the U-mineralizing hydrothermal event.

Within the Placer de Guadalupe mining district, no magmatic rocks record ages are comparable to that of the gold mineralization event (ca. 21 Ma; Fig. 8). This early Miocene age is also an outlier within the regional Eocene to Mio-Pliocene metallogenic history (McDowell and Maugher (1994); Ferrari et al. (2005); Camprubi (2013); Villarreal-Fuentes et al. (2016); Fig. 8). Regional Miocene magmatic activity is limited to the Trans Pecos magmatic domain and the Chihuahua alkalic basalt dyke swarm, which share a structural direction and a relative age range of emplacement (27–24 Ma; K-Ar in whole rocks; Price et al., 1987; Cameron et al., 1989), as well as the recently dated ignimbrite outcrops in western Chihuahua (28–23 Ma; U-Pb in zircon; Mahar et al., 2016). The presence of bimodal magmatism and gold mineralization suggests that an important regional extensional and potential hydrothermal event occurred during the Early Miocene (Figs. 8 and 12A and B).

6.2. U-Mineralizing event

In the PdG district, the late Eocene U-mineralizing event is related to the precipitation of REE-rich calcite, Fe-calcite cements, Fe-oxides and uranium minerals (mostly uraninite). Within different host-rocks throughout the district, the U-hydrothermal event appears to have generated a discrete Fe-oxide dissemination area. Uraninites are not homogeneously disseminated throughout mineralizing veins. Instead, uranium-rich pockets are defined when veins crosscut regions that are rich in organic matter, such as in the middle Jurassic Upper Plomosas sandstone formation and at other stratigraphic levels. In the La Virgen and Puerto del Aire mines, no microthermometric data were obtained from uranium minerals hosted in Fe-calcite cement. However, indicators of mineral paragenesis, such as uranium co-precipitated with REE and Fe-calcite and magnetite (Fig. 7), indicate the presence of fluids with neutral pH and high fO_2, thus suggesting the participation of meteoric fluids. C-O isotopic data obtained from Fe-calcite indicate a process of low thermal alteration involving the participation of "hot fluids" interacting with a relatively shallow Eocene volcanic heat source and Mesozoic limestone host rock during the processes of uranium transport and precipitation (Fig. 10). Sources of U and REE are always complex. Eocene volcanic rocks have been invoked as the sources of the main U deposits in Chihuahua (Goodell, 1981; George-Aniel et al., 1991; Angiboust et al., 2012; Villarreal-Fuentes et al., 2016). The fractionation of the REE has been used to trace geochemical processes associated with hydrothermal activity, including water-rock interaction

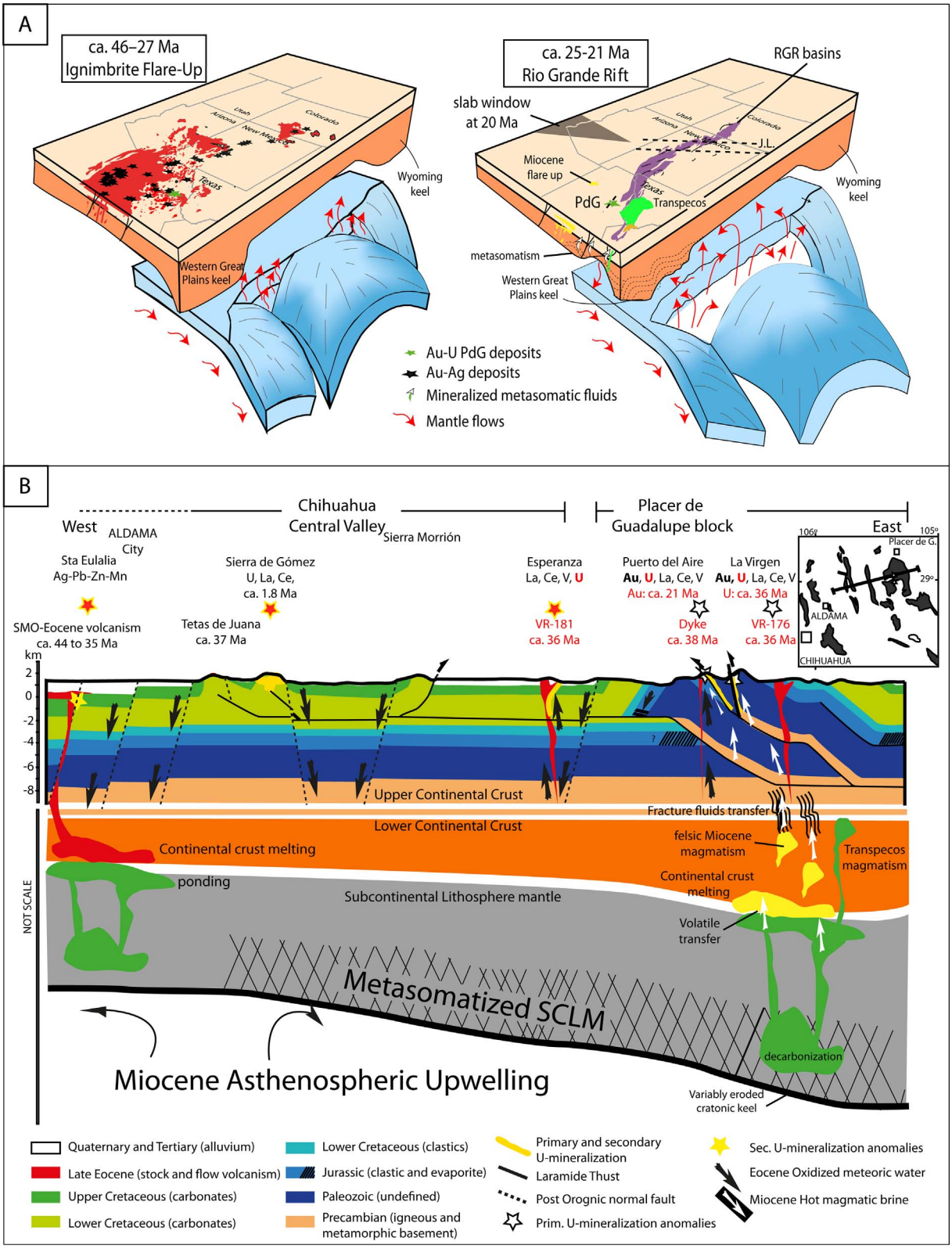

Levresse et al., figure 12

Fig. 12. A) Suggested regional geological model of the genesis of the telescoped Placer de Guadalupe Au-U epithermal deposit (modified de Ricketts et al., 2015). B) Schematic genetic model of the Placer de Guadalupe Au-U deposit. Structural transect is modified from Hennings (1994) and Villarreal-Fuentes et al. (2016).

in hydrothermal systems, the evolution of hydrothermal fluids, degassing of magmatic acid volatiles, mineral precipitation and dissolution. In Fig. 11, the HREE concentration of limestone is 1 and 2 orders of magnitude lower than the REE concentration of the recrystallized limestone and Fe-calcite, respectively, thus suggesting the involvement of other REE-enriched rocks. The few rocks in the Placer de Guadalupe district with high REE concentrations are the Upper Eocene volcanic formations with REE up to 2000 ppm. The carbonatite volcanic event

could present REE up to 23000 ppm (Nandigam et al., 2009). Most acidic fluids from continental geothermal fields have a very distinctive "gull wing" pattern, which has a negative Eu anomaly, although some low-pH hot waters show LREE enrichment and positive or no Eu anomalies. The lack of an Eu anomaly in the Fe-calcite REE pattern suggests that magmatic or volcanic-related fluids were absent in this process (Nozaki et al., 1999; Fig. 11). The Th/U values of ores, minerals and host rocks reflect the oxidation-reduction features of the geological environment (Jones and Manning, 1994): (1) the Th/U value of the oxidizing environment is less than 0.75; (2) Th/U = 0.75–1.25 represents a transitional anoxic environment; (3) the value of Th/U of the reducing environment is > 1.25. The Th/U values of Fe-calcite are lower than 0.75 and vary from 0.14 to 0.28, illustrating relatively strong oxidation of low-pH hot ore-forming fluids. HREE enrichment and high Y/Ho ratios are typical characteristics of a carbonate source (Spier et al., 2007; Franchi et al., 2015). In northern Mexico, the geochemical behavior of the Upper Eocene to Oligocene volcanic sequence suggests that it originated by variable degrees of non-modal partial melting of granulitic low-crustal rocks, which produced chemical disequilibrium during the melting process (McDowell and Mauger, 1994; Orozco-Esquivel et al., 2002; Ricketts et al., 2015). Partial melting is induced by asthenospheric upwelling through crustal break-up and extension (Ricketts et al., 2015). The same geodynamical process increases the generation of magmatism and the thermal anomaly gradient. The Eocene-Oligocene volcanic sequence is characterized by high-silica, peraluminous rhyolites, which are strongly enriched in some incompatible lithophile elements (such as U) and locally ending by carbonatite volcanic formations rich in La and Ce as the U calcite cement event (McDowell and Mauger, 1994; Orozco-Esquivel et al., 2002; Nandigam et al., 2009). The increased Eocene-Oligocene crustal extension allowed meteoric oxidized water to infiltrate along reactivated crustal faults. These heated and oxidized meteoric fluids were efficient at mobilizing the uranium contained in the felsic Eocene volcanic and carbonatitic glass. In summary, the PdG district contained the three necessary conditions to form U-vein deposits: (1) a metal and heat source, represented in this case by late Eocene volcanism and, in particular, a carbonatite volcanic event; (2) an efficient transport mechanism for large-scale meteoric water inputs, which were channeled, heated and U-enriched from a deep U source to a shallow sedimentary chemical trap through reactivated crustal Eocene faults; (3) an effective trap, which is represented here by the reducing conditions front induce by organic matter-rich sedimentary formations. A comparable genetic model was partially suggested for the Peña Blanca U-deposit (Angiboust et al., 2012). The Peña Blanca and PdG deposits formation have comparable age (32–36 Ma), ascending meteoritic fluids as U transport mechanism, Eocene magmatism as U source, and the U precipitation controlled by MO occurrence which inducing redox conditions modification in the mineralizing system. The most significant differences are the stronger tectonic controlled observed in PdG; the host rocks nature, Mesozoic sedimentary and plutonic in PdG versus Eocene volcanic in Peña Blanca; and the emplacement depth and temperature of the mineralizing fluid, higher in PdG. If this genetic model seems to be sufficient to explain the formation of the PdG U-event, it only represents the first stage of the Peña Blanca U-deposit (Angiboust et al., 2012). The wealth of the Peña Blanca U-deposit is related to 30 Ma of reactivations (Angiboust et al., 2012; Villarreal-Fuentes et al., 2016) and U-remobilization events favor by continuous meteoritic oxidized fluids shallow infiltration and microbial reducing activity (Angiboust et al., 2012).

6.3. Au-mineralizing event

The presence of Fe-calcite dissolution, host rock sericitization, calcite REE anomalies and CO_2-rich quartz and calcite cements indicate the participation of more reduced and acidic hydrothermal fluids with a magmatic component in the PdA and LV mines. The C-O isotopic values of white calcite crystals suggest that the carbon has a magmatic origin (Cartigny et al., 1998), and that the fractionation of oxygen follows the trend of low-temperature alteration caused by magmatic-hydrothermal fluids (White and Hedenquist, 1990; Simmons et al., 2005; Fig. 10) as is also seen in U-mineralizing events. The calculated $\delta^{18}O_{H2O}$ values of Au-bearing white calcite from the PdA and LV mines form a line connecting the isotopic values of the local limestone host rocks with those of standard hydrothermal calcite (White and Hedenquist, 1990; Simmons et al., 2005; Lefticariu et al., 2005; Fig. 10); this distribution could be interpreted to reflect either increasing fluid-rock interaction with $\delta^{18}O$-rich wall rocks, or the input of $\delta^{18}O$-rich fluid from an external source. The latter scenario is less likely, because the petrology, Th and salinities of fluid inclusions from the PdA and LV mines show negligible evidence of fluid mixing (Figs. 9 and 10). In addition, the evolution from silicification and sericitization to carbonatization surrounding mineralizing vein alterations in the PdA and LV mines indicate that fluid-rock interaction is a more realistic hypothesis. The REE patterns of white calcite record a decrease in HREE compared to that of the Fe-calcite cement. Hydrothermal fluids enriched in Cl can effectively concentrate light REE but deplete HFSE, whose values of Hf/Sm, Nb/La and Th/La are usually less than 1 (Oreskes and Einaudi, 1990). Besides fluids with an acidic pH are likely more suitable for leaching LREEs during alteration of the host rock or Fe-calcite cement. The leaching of LREEs in the white calcite cement occurred through the dissolution of REE- and Fe-bearing carbonates by acidic hydrothermal solutions and their precipitation during the modification of hydrothermal fluid pH by host-rock interactions (Cantrell and Byrne, 1987). The Au-mineralizing fluids are NaCl-oversaturated and CO_2-rich fluid inclusions (type I and II). Quartz and aqueous white calcite-bearing fluid inclusions range in Th from 217 °C to 305 °C, with homogeneous high salinities ranging from 20 to 39 wt% eq NaCltotal salinity. In PdA, the Type I final fluid inclusions achieve homogenization by halite dissolution, which suggests that they were trapped in liquid-stable and vapor-poor fluids (Cline and Bodnar, 1994) and thus represent the P-T trapping conditions of the mineralizing fluids. If CO_2 traces were detected in Type I fluid inclusions from the PdA quartz and white calcite stages, then no contemporaneous CO_2-bearing or vapor-rich inclusions were observed. Also, in PdA, salinity and the liquid-to-vapor ratio are very homogeneous throughout both time and space. These observations suggest an entrapment of immiscible fluid at P-T conditions below the ebullition level and the absence of a meteoric fluid mixing process (Fig. 9). The arrangement of LV fluid inclusions is more complex, showing an assemblage of CO_2 gas- (type III) and liquid-bearing fluid inclusions with aqueous biphasic fluid inclusions (type II) with lower Th and salinity than Type I PdA fluid inclusions, suggesting different and probably shallower emplacement conditions. Fluid inclusions that homogenize by halite disappearance, as observed in PdA, are common in many hydrothermal ore deposits, including porphyry copper (Bodnar and Beane, 1980), skarn (Baker and Lang, 2003) and iron-oxide copper gold (IOCG; Niiranen et al., 2007) systems, as well as in medium- to high-grade metamorphic environments (Scambelluri et al., 1997). NaCl-oversaturated fluid inclusions can be the result of fluid exsolution from a crystallizing melt or through the immiscibility of aqueous fluids. Coexisting vapor- and liquid-rich fluid inclusions, such as those observed in LV, are generally interpreted as indicators of fluid boiling or immiscibility. Fluid boiling is characterized by (a) petrography (i.e., bladed calcite) (b) different coexisting types of fluid inclusions, (c) contrasting salinity values but similar Th values, (d) coexisting vapor- and liquid-rich fluid inclusions, and (e) heterogeneous L/V ratios. According to the criteria defined by Ramboz et al., 1982, to identify fluid immiscibility, pairs of liquid- and vapor-rich inclusions must: a) demonstrate simultaneous trapping; b) record homogenization temperatures in a comparable temperature range via opposite modes of homogenization; and c) decrepitate in a comparable temperature range if they are similar in size and shape. In LV or PdA, no bladed calcite is observed. The fluid inclusion assemblage in LV show simultaneous

trapping, comparable homogenization temperatures, and homogeneous L/V ratios, suggesting immiscibility. The different homogenization temperatures and the presence of fluid inclusions with comparable densities in LV and PdA suggest that they underwent different evolutions from a unique fluid source. Mineralization in the PdA and LV mines occurs in different fault blocks within the structural thrust stack. Mineralizing fluids are divided at depth; gold-mineralizing brine likely separated from the parental magma at depth, but both ascended during the same time through the reactivated thrust fault system related to the RGR extension. In PdA, the mineralizing brine never reached the ebullition level. In LV, the extension rate was probably higher, which allowed CO_2 degasification to start. The P-T trapping conditions for the gold mineralization event in the PdA mines were calculated using Lecumberri-Sanchez et al. (2012) equations. The Type I fluid inclusions (i.e., the NaCl-oversaturated fluid inclusions in PdA) were trapped at a wide range of pressure (from ca. 130 to 900 bars) and temperature (from 266.6 °C to 305 °C) (Th_{NaCl}) conditions. The minimum thickness of the overlying rocks of the orebodies is estimated to be less than 500 m or ca. 130 bars, which is in good agreement with the known regional geological column (Haenggi, 2001; Villarreal et al., 2014). This difference between lithostatic and fluid pore pressure implies that the mineralizing system in PdA was partially caused by overpressure, which is coherent with the Fe-calcite hydraulic fractures observed in the mineralized veins. The greater relative trapping pressure observed in calcite than quartz suggests that quartz precipitation could have partially sealed the porosity of the host rock and faulted the Fe-calcite cement of this epithermal pulsative system.

Magmatic-hydrothermal Au deposits are usually enriched in many different metals, including S, Cu, Mo, Sb, Bi, W, Pb, Zn, Te, Hg, As, and Ag (Richards, 2009; Phillips, 2013). In gold-only mineralizing districts, such as PdG, three plausible sources have generally been proposed: (1) felsic-intermediate magmas, which release fluids as they crystallize, (2) a hypabyssal magmatic source and (3) metamorphic rocks, from which fluids are generated as temperatures increase (Goldfarb et al., 2005; Phillips and Powell, 2015). Within the PdG district and its close regional area, no evidence of Late Miocene magmatism has been observed to date (Fig. 8). In the Placer de Guadalupe deposits, various gold-only districts do not record coeval magmatic intrusions but do exhibit an important fertile greenschist-facies metamorphic sequence (Wilson et al., 2013). The best source for the generation of auriferous fluids is thus considered to be the greenschist- to amphibolite-facies transition (Elmer et al., 2006). The passage of greenschist-facies rocks to higher metamorphic grade involves devolatilization (2–5 wt% aqueous fluid); the fluid generated is used to mobilize gold and transports it to shallower levels in the crust where the gold may then be precipitated. The determination of the gold sources, presence of NaCl-oversaturated fluids and CO_2-rich immiscible liquids suggest a potential amphibolite source (Fig. 12B). The Late Miocene period in Chihuahua is more closely related to a regional extensional peak than a period of regional metamorphism. However, amphibolite melting could have been induced by magmatic intrusion or by the end of partial melting (enriching the melt in incompatible elements as gold) related to isothermal growth (heating crust). In Central Chihuahua, the Grenvillian basement is composed of *meta*-igneous rocks (1080–1333 Ma, Blount (1993)) and undated amphibolite intruded by trondhjemite, tonalite and granite (Mauger et al., 1983; Fig. 12B). These rocks were exposed to a continually heating crust by magmatic intrusions from the Laramide orogeny, Eocene to Oligocene volcanism (Basin and Range), and an Early Miocene heat pulse from an asthenospheric plume and mantle intrusions (Ricketts et al., 2015; Fig. 12A and B). This anomalous heat flux was amplified by an increasing extensional regime from the Paleocene to the present. The heat propagating through the crust as a consequence of the Laramide and Basin and Range tectonism continued throughout the Rio Grande Rift transition period. This continued heat flow drove the widespread high-temperature low-pressure metamorphism of the crustal amphibolite source rocks during the ideal structural period that liberated the Au-mineralizing fluids and drove them to a shallow crustal level (Fig. 12B).

The factors controlling variations in the ratios of metals within mineralized structures and/or on a district scale can be determined based on petrographic evidence or generally by assuming that Ag and Au undergo cogenetic precipitation. Ag and Au cogenetic precipitation is usually assumed even when the vein texture is characterized by banding and a pulsating hydrothermal system (i.e., in an epithermal low-sulfidation-type deposit). In PdG, as in most of the Ag-Au Mexican low sulfide epithermal deposits, no radioactive dating minerals have been directly linked in areas with high gold concentrations. The ages of the world-class Mexican Oligocene Ag-(Au) deposits have been indirectly determined by K-Ar or ^{40}Ar-^{39}Ar dating in adularia (Camprubi, 2013). Adularia is a characteristic mineral of low-sulfidation epithermal Ag deposits, which is easy to observe in underground deposits and to date by traditional K-Ar or ^{40}Ar-^{39}Ar techniques. However, fluids in Au epithermal deposits are high-sulfidation-type fluids where adularia is rare; therefore, dating is generally performed on sericite or alunite (Sillitoe, 1993). It is possible that dating the most obvious mineral in the world-class Mexican Oligocene Ag-(Au) deposits only reveals one part of its metallogenetic story. The presence of uraninite in the PdG early mineralization event can be used to decipher the telescoped characteristics of the Au-U Placer de Guadalupe epithermal deposit. It allows us to identify a gold Miocene deposit far from they were previously described, in SMO and central Mexico (Ramos Rosique et al., 2011; Mascuñano et al., 2013). This first Miocene gold deposit raises questions about the supposed homogeneity of the world-class Mexican Oligocene Ag-(Au) district and the ways in which we date them. In the Fresnillo/Saucito Au-Ag district, Velador et al. (2010) recorded an adularia argon step-heated spectra from an Au-dominant structure (the Saucito mine). Adularia from the Valdecanas vein records a climbing age spectrum related to hydrothermal alteration (Velador et al., 2010). The authors generally interpreted this analysis to reflect perturbed spectra in which the final step was representative of the crystallization age (ca. 29 Ma), but they did not question the source of the alteration (producing low-temperature ages close to 24 Ma) (Velador et al., 2010). As observed in PdG and in various gold-only epithermal deposits, mineralization is not always spatially related to magmatism and alteration can be discrete (Goldfarb et al., 2005; Phillips and Powell, 2015). In the Valdecañas vein, host-rock sericitization, high Au/Ag ratios and increasing homogenization temperatures could be pertinent proxies for the occurrence of an early Miocene gold mineralization event in the Fresnillo district. Structural and magmatic evidence of punctual Miocene extension are present from the Placer de Guadalupe district in central Chihuahua to the Fresnillo district in Central Mexico (Nieto-Samaniego et al., 2005). Late Oligocene to Miocene mineralization events are locally reported. Mascuñano et al. (2013) presented late Oligocene ages (of ca. 25 Ma) from Re/Os dating of antimonite from the Wadley Sb deposits. Antimonite and gold have comparable geochemical behaviors (Seward, 1993). The new Placer de Guadalupe genetic model represents a new milestone in the metallogenic evolution of central and northern Mexico. It is a necessary to question the genetic model proposed thus far for Ag-Au world class epithermal districts in Mexico, such as those in Fresnillo. In summary, data from the Miocene mineralization in the Fresnillo, Real de Catroce and Placer de Guadalupe deposits indicate that we should remain open to new perspectives regarding the exploration of gold in central and northern Mexico.

7. Conclusions

The Au-U Placer de Guadalupe deposit should be reconsidered as a telescoped epithermal deposit. The deposit's formation occurred during two high-rate extensional events, ca. 36 Ma and ca. 21 Ma, which resulted from a continuous extensional period ca. 50 Ma. Eocene/Oligocene subduction generated high extension rates, which were related to widespread volcanism, mantle wedge metal enrichment and

asthenospheric thinning. These geodynamical conditions allowed the emplacement of high-silica, peraluminous rhyolites, which were strongly enriched in incompatible lithophile elements, as well as U-related deposits, including the Placer de Guadalupe uranium veins. Heated and oxidized meteoric fluids were efficient at mobilizing uranium contained in Eocene felsic volcanic and carbonatitic glass, which then precipitated metals in a shallow, organic matter-rich level of the middle Jurassic upper Plomosas sandstone formation. The Miocene RGR extensional peak, coupled with depleted asthenospheric uplift, facilitated the fusion/metamorphism of the lower crust and the expulsion of large amounts of CO_2-bearing fluids to a shallower crustal level through the reactivated crustal Laramide thrust faults (Fig. 12A). Their interaction with the entire stratigraphic column, from Grenvillian to Late Triassic basement, favored the leaching of gold and the enrichment of CO_2-bearing fluids. Gold deposition was not induced by boiling but was instead caused by water-rock interaction with U mineralization and the Upper Plomosas shale (Fig. 12B).

The Au-U Placer de Guadalupe telescoped epithermal deposit is an outlier in the Mexican epithermal system due to its unusual composition and age. Because the Au-U Placer de Guadalupe deposit is the youngest Mexican gold deposit reported in Central and North Mexico, its genetic relationship with the BnR and RGR transition provides a new perspective regarding the exploration of gold Miocene epithermal deposits in northern Mexico and the southern USA.

Acknowledgments

Special thanks to Marina Vega, Carlos Ortega and Teresa Soledad Medina Malagón for their assistance at the CGEO laboratory. This study was financed by the UNAM-PAPIIT project IN110912 and CONACyT projects 81584 and 80142.

Appendix A. Supplementary data

Supplementary data associated with this article can be found, in the online version, at http://dx.doi.org/10.1016/j.oregeorev.2017.10.011.

References

Alba, L.A., Chavez, R., 1974. K-Ar ages of volcanic rocks from the central Sierra Peña Blanca, Chihuahua, Mexico. Isochron West 10, 21–23.
Angiboust, S., Fayek, M., Power, I., Camacho, A., Calas, G., Southam, G., 2012. Structural and biological control of the cenozoic epithermal uranium concentrations from the Sierra Peña Blanca, Mexico. Miner. Depos. 47, 859–874.
Aranda-Gomez, J.J., Luhr, J.H., Housh, T.B., Connor, C.B., 2003. Synextensional Pliocene– Pleistocene eruptive activity in the Camargo volcanic field, Chihuahua, Mexico. Geol. Soc. Am. Bull. 115, 298–313.
Averil, M.G., Miller, K.C., 2013. Upper crustal structure of the southern Rio Grande rift: a composite record of the rift and pre rift tectonic. Geol. Soc. Am. Spec. Pap. 494, 463–474.
Baker, T., Lang, J.R., 2003. Reconciling fluid inclusions, fluid processes and fluid source in skarns: an example from the Bismark skarn deposit, Mexico. Miner. Depos. 38, 474–495.
Baldridge, W.S., Olsen, K.H., Callender, J.F. 1984. Rio grande rift: problems and perspectives. New Mexico geological society guidebook, 35th Field Conference, Rio Grande Rift, Northern New Mexico.
Bartolino, J.R., 1992. Modified basin and range topography in the Bolson de Mapimi, Durango and Chihuahua, Mexico. TEX J. Sci. 44, 295–300.
Blount, J.G. 1993. The geochemistry, petrogenesis, and geochronology of the Precambrian meta-igneous rocks of Sierra del Cuervo and Cerro El Car- rizalillo, Chihuahua, Mexico (Ph.D. dissertation), Austin, University of Texas at Austin, pp. 242.
Bodnar, R.J., Beane, R.E., 1980. Temporal and spatial variations in hydrothermal fluid characteristics during vein filling in preore cover overlying deeply buried porphyry copper type mineraliz- ation at Red Mountain, Arizona. Econ. Geol. 75, 876–893.
Boiron, M.C., Cathelineau, M., Banks, D.A., Fourcade, S., Vallance, J., 2003. Mixing of metamorphic and surficial fluids during the uplift of the Hercynian upper crust: consequences for gold deposition. Chem. Geol. 194, 119–141.
Bridges, L.W., 1962. Geology of Mina Plomosa area, Chihuahua, Mexico, Austin, Texas. PhD thesis, University of Texas at Austin.
Cantrell, K.J., Byrne, R.H., 1987. Rare earth element complexation by carbonate and oxalate ions. Geochem. Cosmochem. Acta 51, 597–605.
Cameron, K.L., Nimz, G.J., Niemeyer, S., Gunn, S., 1989. Southern Cordilleran basaltic andesite suite, southern Chihuahua, Mexico: a link between Tertiary continental arc and flood basalt magmatism in North America. J. Geophys. Res. 94 (B6), 7817–7840.
Campa, M.F., Coney, P.J., 1983. Tectonostratigraphic terranes and mineral resource distributions in Mexico. Can. J. Earth Sci. 20 (6), 112–135.
Camprubi, A., Albinson, T. 2007. Epithermal deposits in Mexico – Update of current knowledge, and an empirical reclassification, In: Alaniz-Alvarez, S.A., Nieto-Samaniego, A.F. (Eds.), Geology of Mexico: Celebrating the Centenary of the Geological Society of Mexico, Geological Society of America Special Paper 422, 377–415.
Camprubí, A., 2013. Tectonic and metallogenic history of Mexico. Soc. Econ. Geol. Spec. Publ. 17, 201–243.
Harris, J.W., Philips, D., Girard, M., Javoy, M., 1998. Subduction-related diamonds ? – the evidence for a mantle derived origin from coupled d13C–d15N determinations. Chem. Geol. 147–159.
Clark, K.F., Fitch, D.C., 2005. Distribution of Mid-Miocene to Recent metallization in Mexico, en R. Corona-Esquivel, y J.A. Gómez-Caballero, (Eds.), Acta de Sesiones: Asociación de Ingenieros de Minas, Metalurgistas y Geólogos de Mexico, XXVI Convención Internacional de Minería, pp. 20–30.
Clark, K.F., Fitch, D.C. 2009. Evolución de los depósitos metálicos en el tiempo y espacio en Mexico. In: Clark, Kenneth F., Salas-Piza, Guillermo A., Cubillas-Estrada, R. (Eds.), Geologia Economica de Mexico, second ed. Asociación de Ingenieros de Minas, Metalurgistas y Geólogos de Mexico, Servicio Geologico Mexicano, pp. 62–133.
KF, Clark, Salas, GA, 1988. A special issue devoted to the geology and mineral deposits of Mexico. Econ. Geol. 83 (8), 1493–2001.
Clark, K.F. 1997. Mineral Deposit Evolution in Time and Space in Mexico: Universidad Nacional Autonoma de México, Instituto de Geologia II Convencion sobre la Evolucion Geologica de México y Recursos Asociadas, Simposio y Coloquio, pp. 281–284.
Cline, J.S., Bodnar, R.J., 1994. Direct evolution of a brine from a crystallizing silicic melt at the Questa, New Mexico, molybdenum deposit. Econ. Geol. 89, 1780–1802.
Cuney, M., Friedrich, M., Blumenfeld, P., Bourguignon, A., Boiron, A.C., Vigneresse, J.L., Poty, B., 1990. Metallogenesis in the French part of the Variscan orogen. Part I: U preconcentrations in pre-Variscan and Variscan formation – a comparison with Sn W and Au. Tectonophysics 177, 39–57.
De Cserna, Z., Rincon-Orta, A., Solorio-Murguía, C., Schmitter, V., 1968. Una edad radiométrica Pérmica temprana en la región de Placer de Guadalupe, noreste de Chihuahua. Bol. Soc. Geol. Mex. 31, 65–73.
Domeier, M., Torsvik, T.H., 2014. Plate tectonics in the late Paleozoic. Geosci. Front. 5, 303–350.
Drewes, H.D., 1981. Tectonics of southeastern Arizona: USGS Professional Paper 1144.
Elmer, F.L., White, R.W., Powell, R., 2006. Devolatilisation of metabasic rocks during greenschist-amphibolite facies metamorphism. J. Metamorph. Geol. 24, 497–513.
Enriquez, E., Rivera, R. 2001. Timming and magmatic hydrothermal activity in the San Dimas District, Durango, Mexico. Soc. Econ. Geol., SP8, 33–38.
Fayek, M., Kyser, K., 1997. Characterization of multiple fluid-flow events and rare-earth-element mobility associated with the formation of unconformity-type uranium deposits in the Athabasca Basin, Saskatchewan. Can. Min. 35, 627–658.
Fayek, M., Ren, M., Goodell, P., Dobson, P., Saucedo, A.L,, Kelts, A., Utsunomiya, S., Ewing, R.C., Riciputi, L.R., Reyes, I., 2006. Paragenesis and geochronology of the Nopal I uranium deposit, Mexico. In: 11th International High Level Radioactive Waste Management Conference Proc., Las Vegas, NV, pp. 55–62.
Ferrari, L., Valencia-Moreno, M., Bryan, S. 2005. Magmatismo y tectónica en la Sierra Madre Occidental y su relación con la evolución de la margen occidental de Norteamérica. Boletin de la Sociedad Geológica Mexicana, Tomo LVII, n. 3.
Finch, R.J., Murakami, T., 1999. Systematics and paragenesis of uranium minerals. In: Burns, P.C., Finch, R.J., (Eds.), Uranium: mineralogy, geochemistry, and the environment. Mineralogical Society of America, Reviews in Mineralogy 38. Washington, USA.
Franchi, F., Hofmann, A., Cavalazzi, B., Wilson, A., Barbieri, R., 2015. Differentiating marine vs hydrothermal processes in Devonian carbonate mounds using rare earth elements (Kess Kess mounds, Anti-Atlas, Morocco). Chem. Geol. 409, 69–86.
George-Aniel, B., Leroy, J., Poty, B., 1991. Volcanogenic uranium mineralizations in the Sierra Peña Blanca district, Chihuahua, Mexico: three genetic models. Econ. Geol. 86 (2), 233–248.
Gilmer, A.L., Clark, K.F., Conde, J.C., Hernandez, I.C., Figueroa, J.I., Porter, E.W., 1988. Sierra de Santa Maria, Velardeña mining district, Durango, Mexico. Econ. Geol. Bull. Soc. Econ. Geol. 83, 1802–1829.
Goldfarb, R.J., Baker, T., Dube, B., Groves, D.I., Hart, C.J.R., Gosselin, P. 2005. Distribution, character, and genesis of gold deposits in metamorphic terranes. In: Hedenquist, J.W., Thompson, J.F.H., Goldfarb, R.J., Richards, J.P., (Eds.), Economic Geology. 100th Anniversary Volume 1905–2005. Littleton, Colorado, Society of Economic Geologists, pp. 407–450.
Goodell, P.C., 1981. Geology of the Peña Blanca uranium deposits, Chihuahua, Mexico. In: Goodell, P.C. Waters, A.C. (Eds.), Uranium in Volcanic and Volcanoclastic Rocks – AAPG Studies in Geology No. 13, American Association of Petroleum Geologists, pp. 275–291.
Goodell, P.C., Feinstein, N.M., 2008. A simulated 43-101 document of the Plomosa Property: Chihuahua, Mexico: Reporte para Compañia Retec Guaru, S.A. de C.V., pp. 36.
Gonzales Reyna, J., 1946. Los criaderos de uranio y oro en Placer de Guadalupe y Puerto del Aire, estado de Chihuahua: Boletin del Consejo de recursos Naturales No Renovables, Mexico. 5, pp. 235.
González-Reyna, J., 1956. Memoria Geológico-Minera del Estado de Chihuahua (Minerales Metálicos), en XX Congreso Geológico Internacional, México, D.F., pp. 280.
Haenggi, W.T., 2002. Tectonic history of the Chihauhua trough, Mexico and adjacent USA, part II: Mesozoic and Cenozoic. Boletin de la Sociedad Geologica Mexicana, LV,

1, 38–94.
Haenggi, W.T., 2001. Tectonic history of the Chihuahua trough, Mexico and adjacent USA, Part I: the preMesozoic setting: Boletín de la Sociedad Geológica Mexicana, LIV, pp. 28–66.
Hall, B.V., Behnam, B., Jakubowski, W., Vila-Sanchez, A.R., Diaz-Martinez. R., Gorzynski, G.A., 2014. Intergrating five hundred years of geological information in the search for new mines, Real de minas de Zacualpan district, Central Mexico. 2014 GSA Annual Meeting in Vancouver, British Columbia (19–22 October 2014) n° 205–207.
Hayba, D.O., Bethke, P.M., Heald. P., Foley. N.K., 1985. Geologic, mineralogic and geochemical characteristics of volcanic-hosted epithermal precious-metal deposits. In: Berger, B.R., Bethke, P.M. (Eds.), Geology and Geochemistry of Epithermal Systems: Littleton, Reviews in Economic Geology, 2, 129–167.
Henderson. P., 1984. Rare Earth Elements Geochemistry. Developments in Geochemistry. Elsevier, Amsterdam 2: 510.
Hennings, P.H., 1994. Structural transect of the southern Chihuahua fold belt Between Ojinaga and Aldama, Chihuahua, Mexico. Tectonics 13, 1445–1460.
Herrera-Monreal, J.C., 2011. Analisis de las condiciones metalogeneticas del yacimiento de Uranio "La Coma Buenavista" en el noreste de Mexico, Universidad Autonoma de Nuevo Leon, (unpublished Msc Thesis), pp. 207.
Humphreys, E.D., 1995. Post-Laramide removal of the Farallon slab, western United States. Geology 23, 987–990.
Hynes, S.E., 1999. Geochemistry of Tertiary Epithermal Ag–Pb–Zn Veins in Taxco, Guerre- ro, Mexico. Unpublished M. Sc. Thesis, Laurentian University, Sudbury, Ontario, Canada, pp. 158.
Ingersoll, R.V., Schweicker, R.A., 1986. A plate-tectonic model for Late Jurassic Ophiolite Genesis, Nevadan orogeny and forearc initiation, northern California. Tectonics 5, 901–912. http://dx.doi.org/10.1029/TC005i006p00901.
Iriondo, A., Kunk, M.J., Winick, J.A., Consejo de Recursos Minerales. 2004. $^{40}Ar/^{39}Ar$ dating studies of minerals and rocks in various areas in Mexico: USGS/CRM Scientific Collaboration (Part II): U.S. Geological Survey Open File Report, OF-04-1444, pp. 46.
Jones, B., Manning, D.A.C., 1994. Comparison of geochemical indices used for the interpretation of palaeoredox conditions in ancient mudstones. Chem. Geol. 111, 111–129.
King, R.E., Adkins, W.S., 1946. Geology of a part of the lower Conchos Valley, Chihuahua, Mexico. Bull. Geol. Soc. Am. 57, 275–294.
Klinkhammer, G.P., Elderfield, H., Edmond, J.M., Mitra, A., 1994. Geochemical implications of rare earth element patterns in hydrothermal fluids from mid-oceanic ridges. Geochim. Cosmochim. Acta 58, 5105–5113.
Koděra, P., Lexa, J., Rankin, A.H., Fallick, A.E., 2005. Epithermal gold veins in a caldera setting: Banská Hodruša, Slovakia. Miner. Depos. 39, 921–943.
Krieger, P., 1932. An association of gold and Uraninite from Chihuahua, Mexico. Econ. Geol. 27, 651–660.
Lecumberri-Sanchez, P., Steele-MacInnis, M., Bodnar, R.J., 2012. A numerical model to estimate trapping conditions of fluid inclusions that homogenize by halite disappearance. Geochim. Cosmochim. Acta 92, 14–22.
Lefticariu, L., Perry, E.C., Fischer, M.P., Banner, J.L., 2005. Evolution of fluid compartmentalization in a detachment fold complex. Geology 33, 69–72.
Ludwig, K., 2008. Isoplot/EX version 3.0, A Geochronological Toolkit for Microsoft Excel, Berkeley Geochronology Center Special Publication.
Mahar, A.M., Goodell, P.C., Feinstein, M.N., 2016. Tectono-magmatic evolution of the Chihuahua-Sinaloa border region in northern Mexico: insights from zircon-apatite U-Pb geochronology, zircon Hf isotope composition and geochemistry of granodiorite intrusions. Lithos 264, 555–576.
Mango, H., Arehart, G., Oreskes, N., Zantop, H., 2014. Origin of epithermal Ag-Au-Cu-Pb-Zn mineralization in Guanajuato, Mexico. Miner. Depos. 49, 119–143.
Mauger, R.L., McDowell, F.W., Blount, J.G., 1983. Grenville-age Precambrian rocks of the Los Filtros area near Aldama, Chihuahua, Mexico. In: Clark, K.F., Goodell, P.C. (Eds.), Geology and mineral resources of north-central Mexico, El Paso Geological Society, Field Conference Guidebook, pp. 165–168.
Mascuñano, E., Levresse, G., Reisberg, L., Tritlla, J., Cardellach, E., Corona-Esquivel, R., 2013. New Re/Os ages for the Wadley Sb deposits, Mesa Central Mexico: metalogenic implications. XXX Convención Internacional de Minería 2013. Acapulco 2013. Mundo Imperial 16 al 19 de Octubre 2013 Acapulco Guerrero, México. ISBN 978-607-95292-6-0.
McCrea, J.M., 1950. On the isotopic chemistry of carbonates and a paleotemperature scale. J. Chem. Phys. 18, 849–857.
McDowell, F.W., Roldán-Quintana, J., Amaya-Martínez, B., 1997. Interrelationship of sedimentary and volcanic deposits associated with tertiary extension in Sonora, Mexico. Geol. Soc. Am. Bull. 109, 1349–1360.
McDowell, F.W., Maugher, R.L., 1994. K-Ar and U-Pb zircon chronology of late cretaceous and tertiary magmatism in central Chihuahua State, Mexico. Geol. Soc. Am. Bull. 106, 118–132.
McIntosh, A.N., 2004. Stable Isotopic Evidence for Fluid Mixing in the Tertiary Alkali-Type Epithermal Au-Te deposit Cripple Creek, CO. New Mexico Institut of Minning Technology, pp. 124 (Msc Thesis).
McLemore, V.T., 2011. The grants uranium district, New Mexico: update on source, deposition, and exploration. Montana Geol. 48, 23–44.
McLemore, V.T., North, R.M., 1984. Occurrences of precious metals and uranium along the Rio Grande rift in northern New Mexico. In: Baldridge, W.S., Dickerson, P.W., Riecker, R.E., Zidek, J. (Eds.), Rio Grande Rift (Northern New Mexico). New Mexico Geological Society 35th Annual Fall Field Conference Guidebook, pp. 205–212.
Megaw, P.K.M., Ruiz, J., Titley, S.R., 1988. High-temperature, carbonate-hosted Ag-Pb-Zn (Cu) deposits of northern Mexico. Econ. Geol. 83, 1856–1885.
Moncada, D., Mutchler, S., Nieto, A., Reynolds, J., Rimstidt, J.D., Bodnar, R.J., 2012. Mineral textures and fluid inclusion petrography of the epithermal Ag-Au deposits at Guanajuato, Mexico: application to exploration. J. Geochem. Explor. 114, 20–35.
Mosher, S., 1998. Tectonic evolution of the southern Laurentian Grenville orogenic belt. Geol. Soc. Am. Bull. 110 (11), 1357–1375.
Nandigam, R., Clark, K.F., Anthony, E.Y., Comaduran-Ahumada, O., 2009. Características geológicas y geoquímicas de un complejo carbonatitico enriquecido en Zn y LREE del Terciario de Chihuahua septentrional, México. In: Kenneth, F., Clark, Guillermo, A., Salas-Pizá, Rodolfo Cubillas-Estrada (Eds.), Geologia Económica de Mexico, second ed. Asociación de Ingenieros de Minas, Metalurgistas y Geólogos de México, Servicio Geológico Mexicano, pp. 506–516.
Nieto-Samaniego, A.,F, Alaniz-Álvarez, A., Camprubí Cano, A. 2005. La Mesa Central de México: estratigrafía, estructura y evolución tectónica cenozoica, en Nieto-Samaniego, A. F., Alaniz-Álvarez, S. A. (Eds.), Temas selectos de la Geología Mexicana: Boletín de la Sociedad Geológica Mexicana, Volumen Conmemorativo del Centenario, 57, 3, pp. 285–317.
Niiranen, T., Poutiainen, M., Mänttäri, I., 2007. Geology, geochemistry, fluid inclusion characteristics, and U-Pb age studies on iron oxide–Cu–Au deposits in the Kolari region, northern Finland. Ore Geol. Rev. 30, 75–105.
Nozaki, Y., Alibo, D.S., Amakawa, H., Gamo, T., Hasumoto, H., 1999. Dissolved rare earth elements and hydrography in the Sulu Sea. Geochim. Cosmochim. Acta 63, 2171–2181.
Ohmoto, H., Rye, R.O. 1979. Isotope of sulfur and carbon. In: Barnes, H.L. (Ed.), Geochemestry of Hydrothermal deposits, John Wiley & Sons, pp. 509–567.
Oreskes, N., Einaudi, M.T., 1990. Origin of rare-earth element enriched hematite breccias at the Olympic Dam Cu-U-Au-Ag deposit, Roxby Downs, South Australia. Econ. Geol. Bull. Soc. Econ. Geol. 85, 1–28.
Orozco-Esquivel, M.T., Nieto-Samaniego, A.F., Alaniz-Alvarez, S.A., 2002. Origin of rhyolitic lavas in the Mesa Central, Mexico, by crustal melting related to extension. J. Volcanol. Geotherm. Res. 118, 37–56.
Oviedo-Patron, E.G., Aranda-Gomez, J.J., Chavez-Cabello, G., Milona-Garza, R.S., Iriondo, A., Gonzalez-Becerra, P.C., Cervantes-Corona, J.A., Solorio-Munguia, J.G., 2010. Tectónica de la sierra Cuesta El Infierno y su posible relación con fallas reactivadas cerca del levantamiento de Plomosas, Chihuahua, México. Rev. Mex. Cienc. Geol. 27 (3), 389–411.
Phillips, G.N., Powell, R. 2015. A practical classification of gold deposits, with a theoretical basisOre. Geology Reviews, 65, 568–573.
Phillips, G.N. 2013. Australian and global setting for gold. In: Proceedings World Gold 2013, Brisbane, Australia, 26–29 September, 2013: The Australian Institute of Mining and Metallurgy, pp. 15–21.
Pinto-Linares, P.J., Levresse, G., Jordi Tritlla, J., Valencia, V.A., Torres-Aguilera, J.M., González, M., Estrada, D., 2008. Transitional adakite-like to calc-alkaline magmas in a continental extensional setting at La Paz Au-Cu skarn deposits, Mesa Central, Mexico: metallogenic implications. Rev. Mex. Cienc. Geol. 25, 39–58.
Price, J.G., Henry, C.D., Barker, D.S., Parker, D.F. 1987. Alkalic rocks of contrasting tectonic settings in Trans-Pecos Texas, Spec. Pap. Geol. Soc.Am., 215, 335–346.
Ramboz, C.l., Pichavant, M., Weisbrod, A. 1982. Fluid immiscibility in natural processes: use and misuse of fluid inclusion data, II. Interpretation of fluid inclusiop. data in terms of immiscibility. In: Kreulen, R., Touret, J. (Guest-Editors), Curreni Research on Fluid Inclusions. Chemical Geology, 37, 29–48.
Ramos-Rosique, A., Bryan, S., Ferrari, L., Lopez Martinez, M., Rankin, A., Camprubi, A., Allen, C., Uysal, T., Feng, Y., Reiners, P. 2011 Chronology of mid-Cenozoic magmatism and epithermal mineralization in the Bolaños graben, southern Sierra Madre Occidental, Mexico. 11th SGA meeting, Let's Talk ore deposits, 26–29 september, Antofagasta, Chile, 139–141.
Ramos-Rosique, A. 2013. Timing and evolution of late Oligocene to early Miocene magmatism and epithermal mineralization in the Bolanos Graben, southern Sierra Madre Occidental, Mexico. (PhD thesis), Kingston University, pp. 213.
Ray, J.S., Ramesh, R., Pande, K., 1999. Carbon isotopes in Kerguelen plume-derived carbonatite: evidence for recycled inorganic carbon. Earth Planet. Sci. Lett. 170, 205–214.
Reyes-Cortés, M., Reyes-Cortés, I.A., Espino-Valdez, S., Rentería-Villalobos, M., Burillo-Montúfar, J.C., Montero-Cabrera, M.E., 2012. Origen and distribution of the natural radioactivity in the northern part of the Chihuahua basin, Mexico. Rev. Mex. Cienc. Geol. 29, 659–675.
Reyes-Cortés, M., Fuentes-Cobas, L., Torres-Moye, E., Esparza-Ponce, H., Montero-Cabrera, M., 2010. Uranium minerals from the San Marcos District, Chihuahua, Mexico. Mineral. Petrol. 99, 121–132.
Ricketts, J.W., Kelley, S.A., Karlstrom, K.E., Schmandt, B., Donahue, M.S., van Wijk, J. 2015. Synchronous opening of the Rio Grande rift along its entire length at 25–10 Ma supported by apatite (U-Th)/He and fission-track thermochronology, and evaluation of possible driving mechanisms. Geological Society of America Bulletin, B31223. 1-28.
Richards, J.P., 2009. Postsubduction porphyry Cu-Au and epithermal Au deposits: products of remelting of subduction-modified lithosphere. Geology 37, 247–250.
Rocha-Rocha, M., 2016. Metallogenesis of the Peñasquito polymetallic deposit: a contribution to the understanding of the magmatic ore systeme. Unpublished PhD thesis, University of Nevada, Reno, pp. 310.
Scambelluri, M., Piccardo, G.B., Philippot, P., Robbiano, A., Negretti, L., 1997. High salinity fluid inclusions formed from recycled seawater in deeply subducted alpine serpentinite. Earth Planet. Sci. Lett. 148, 485–500.
Simmons, S.F., White, N.C., John, D.A. 2005. Geological characteristics of epithermal precious and base metal deposits. In: Economic Geology 100th Anniversary Volume, 485–522.
Sillitoe, R.H. 1993. Epithermal models: genetic types, geometrical controls and shallow features. In: Kirkham, R.V., Sinclair, W.D., Thorpe, R.I., Duke, J.M. (Eds.), Mineral Deposit Modeling: Toronto, Geological Association of Canada, Special Paper, 40, pp. 403–417.
Solari, L.A., Gómez-Tuena, A., Bernal, J.P., Pérez-Arvizu, O., Tanner, M., 2010. U-Pb

zircon geochronology with an integrated LA-ICP-MS microanalytical workstation: achievements in precision and accuracy. Geostand. Geoanal. Res. 34 (1), 5–18.
Solé, J., 2009. Determination of K-Ar ages in milligram samples using an infrared laser for argon extraction. Rapid Commun. Mass Spectrom. 23, 3579–3590.
Solé, J., Enrique, P., 2001. X-ray fluorescence analysis for the determina- tion of potassium in small quantities of silicate minerals for K-Ar dating. Anal. Chim. Acta 440, 199–205.
Spier, C.A., Oliveira, S.M., Sial, A.N., Rios, F.J., 2007. Geochemistry and genesis of the banded iron formations of the Cauê Formation, Quadrilátero Ferrífero, Minas Gerais, Brazil. Precambr. Res. 152, 170–206.
Steele-MacInnis, M., Lecumberri-Sanchez, P., Bodnar, R.J., 2012. HOKIEFLINCS_H_2O-NACL: a Microsoft Excel spreadsheet for interpreting microthermometric data from fluid inclusions based on the PVTX properties of H_2O–NaCl. Comput. Geosci. 49, 334–337.
Steiger, R.H., Jager, E., 1977. Subcommission on geochronology: convention on the use of decay constants in geo- and cosmochronology. Earth Planet. Sci. Lett. 36 (3), 359–362.
Stern, R.J., Dickinson, W.R., 2010. The Gulf of Mexico is a Jurassic backarc basin. Geosphere 6, 739–754.
Sun, S.S., McDonough, W.F. 1989. Chemical and isotopic processes in basaltimplications for mantle composition and processes. In: Saunders, A.D., Norry, M.J. (Eds.), Magmatism in the ocean basins, Geological Society of London, London, 42, pp. 313–345.
Taylor, H.P., Frechen, J., Degens, E.T., 1967. Oxygen and carbon isotope studies of carbonatites from the Laacher See district, West Germany and the Alnö district, Sweden. Geochim. Cosmochim. Acta 31, 407–430.
Torres, R., Ruiz, J., Patchett, P.J., Grajales, J.M. 1999. Permo-Triassic continental arc in eastern México: Tectonic implications for reconstructions of southern North America. In: Bartolini, C., Wilson, J.L., Lawton, T.F. (Eds.), Mesozoic Sedimentary and Tectonic History of North-Central Mexico. Geological Society of America, Special Paper 340, pp. 191–196.
Tosdal, R., Dills, J.H., Cooke, D., 2009. From source to sinks in auriferous magmatic-hydrothermal porphyry and epithermal deposits. Elements 5, 289–295.
Velador, J.M., Heizler, M.T., Campbell, A.R., 2010. Timing of magmatic activity and mineralization and evidence of a long-lived hydrothermal system in the Fresnillo silver district, Mexico: constraints from $^{40}Ar/^{39}Ar$ geochronology. Econ. Geol. 105, 1335–1349.
Vidal, C.P., Guido, D.M., Jovic, S.M., Bodnar, R.J., Moncada, D., Melgarejo, J.C., Hames, W. 2016. The Marianas-San Marcos vein system: characteristics of a shallow low sulfidation epithermal Au–Ag deposit in the Cerro Negro district, Deseado Massif, Patagonia, Argentina. Mineralium Deposita, pp. 1–24.
Villarreal, J., Levresse, G., Nieto-Samaniego, A., Corona-Esquivel, R., 2014. New geological and geochronological data of the Placer de Guadalupe uplift, Mexico: a new piece of the Jurassic Nazas Arc? Int. Geol. Rev. 56 (16), 2000–2014.
Villarreal-Fuentes, J., Levresse, G., Nieto-Samaniego, A.F., Alexandre, P., Corona-Esquivel, R., 2016. Geochemistry and geochronology of the Sierra de Gomez Limestone-hosted U deposit, Chihuahua: implications for distribution of Rio Grande rift mineral deposits in northern Mexico. Ore Geol. Rev. 76, 19–34.
Wells, R.C., 1930. Uraninite from Placer de Guadalupe, Chihuahua. Am. Mineral. 15, 470–473.
White, N.C., Hedenquist, J.W., 1990. Epithermal environments and styles of mineralization: variations and their causes, and guidelines for exploration. J. Geochem. Explor. 35, 445–474.
Wilson, C.J.L., Schaubs, P., Leader, L.D., 2013. Mineral precipitation in the quartz reefs of the Bendigo gold deposit, Victoria, Australia. Econ. Geol. Bull. Soc. Econ. Geol. 108, 259–278.
Zheng, Y.F., 1999. Oxygen isotope fractionation in carbonate and sulfate minerals. Geochem. J. 33, 109–126.